&

DEVELOPMENT OF ANKLE-FOOT ORTHOSIS DESIGN

Presented to: Dr. Paul Labossiere, P. Eng, William Hadi, CO(c), Dr. Sean O'Brien, P.Eng.
Date: 12/06/2017

Matt Wallis

Alanna Gray

Branden Little

Zaid Albiaty

MECH 4860 – University of Manitoba – Mechanical Engineering

EXECUTIVE SUMMARY

This report outlines the final design process for the Ankle-foot orthosis (AFO) in partnership with Anderson Orthopedics. The project objective was to create an AFO prototype that aimed to compensate for muscle weakness in gait, and maximize forward propulsion, while providing quantifiable justification of critical design choices.

The first section of the report details the concept generation phase. In this phase, the needs of the client and patient were first determined. Our team then generated 21 concepts, which were narrowed down to four main options. Then a kinematic and dynamic model was generated to determine the target stiffness of the AFO, which had a value of 1.4 Nm/deg. Then, the safety factor of the AFO was determined to be 2.52 and the final material was determined to be Windform SP. The last section of the concept generation was to create 3D models of the four main concepts using CanFit, to input into Hyperworks for optimization.

The second section of the report pertains to specific design details. The optimization process was conducted for the two most desirable concepts, an optimized version of the pre-existing prototype, and a posterior strut design. It was then determined that the lateral strut design was infeasible due to excessive lateral bending during gait. From this, it was determined that the functionality needs could only be met by a design iterating upon a posterior strut concept. The final design had an achieved height of 38.1cm, width of 9.5cm, length 27.8cm, and weight of 575g. The linear stiffness attained was 1.88N/mm, and overall bending stiffness 4.01Nm/degrees. The approximate cost to manufacture the device was about $3000 USD. Given the limited design space, a design was achieved utilizing an attained stiffness of 4.1 Nm/deg. The achieved FOS was 1.33 as detailed by stress contour results. These numbers deviate in some magnitude from the targets sought out at the onset of the project, but the overall goal of proving feasibility of 3D printing for this specific application was achieved, and the device produced should in theory provide quantifiable benefits to the specific patient’s gait.

TABLE OF CONTENTS

TABLE OF FIGURES

LIST OF TABLES

1 INTRODUCTION

This document outlines the process and final results of developing an Ankle-Foot Orthoses (AFO) with the support of Anderson Orthopedics. A brief background is given followed by the problem statement and formalized project objectives. The Design Procedure section begins with a summary of the preliminary design phase, including customer needs and project constraints, followed by initial patient testing. The conceptual design phase is covered next as we outline the preliminary brainstorming process and final concept selection. The detailed analysis phase includes a kinematic and dynamic analysis of patient test data, the determination of an appropriate safety factor, FMEA and fatigue analyses, material selection and a DFAM plan. Additionally, the model is prepared for optimization using CANFIT and Geomagics. Lastly, the detailed design section explains the rigorous optimization process that lead to our final design and recommendations are provided.

1.1 BACKGROUND INFORMATION

Ankle-foot orthoses (AFO) are used for physical limitations of the lower leg. AFOs can be prescribed as a persistent corrective device that provides a combination of rigidity and spring-back to compensate for the reduced muscle activity. The energy transfer from muscles through connective tissue to the bone requires that all components can sustain the required stress, and the entire joint behaves like a mechanical linkage with a series of actuators providing power input. AFOs can be used to aid the leg when the limited flexion requires a modified pattern of motion.

To understand how the described locomotive limitations can be treated, one must understand the human gait cycle. Gait is the cyclic, mostly repetitive motion humans exhibit when they walk. The pattern of this motion is specific to each individual and tends to naturally expend the least amount of effort.

Gait happens in the two distinct phases distinguished below:
1. Stance phase: The foot contacts ground and ground reaction force transmits at variable magnitude and direction through the foot to counteract the downward pointing net weight of the body.

2. Swing phase: The foot enters into and enacts an aerial stride wherein the only forces transmitted through the leg are inertial.

These phases occur in an overlapping fashion wherein the load bearing activity of each individual leg can be characterized as being either:
1. Double Support: Heel contacts ground, until opposite foot toes leave ground, load is shared in some ratio between legs.
2. Single Support: Opposite foot is now completely off the ground, and until it again contacts the ground, the initial leg supports the entirety of the load.

Figure 1 - Single and Double Support Stages of Gait [2]

One foot supports the entire load in the single support portion, and lasts the majority of the gait cycle. The weight transfer across the pad of the foot is progressive and non-linear in this region, which adds a level of complexity to analyzing the body's dynamics. For this reason, the single support foot load is commonly quantified using multiple degree-of-freedom force plates. With knowledge of this weight transfer, one can start to understand the relationship between patient weight and muscle actuation.

Muscles actuate the limbs through fiber contraction. This generates tension, which provides the muscle force that a motion requires. One muscular limitation that an AFO can be designed to help assist with is the flexion of the foot, both in the dorsal direction

(upwards away from the limb extremity) and the plantar direction (downward, towards the extremities). These actuations occur as a conjunctive effort of muscles extending from the toes up the calf. When one of these muscles cannot provide adequate force, the others must compensate so that the sum of all provided forces is the desired motion that the nervous system is signaling.

As a person shifts their weight to facilitate the motion of their legs, their center of mass will adjust, as will the distribution of pressure along the sole of the foot bearing the reaction load. This ground reaction force (GRF) is vectored in the direction of the center of mass. Therefore, depending on where center of mass is located along the sagittal plane (using an anatomical coordinate system) at any given time when a foot is contacting the ground, a moment will be produced by the distance between the patient's center of mass (COM) and the resultant vector of the GRF. To maintain stability, this moment must be counteracted by flexion in the joints. In Figure 2, the distance between the GRF and the knee joint is shown. The joint must flex to counteract the resulting moment. Flexing the joint is necessary for balance, but can become problematic when foot muscle weakness places the GRF at distances that cause a person's gait to

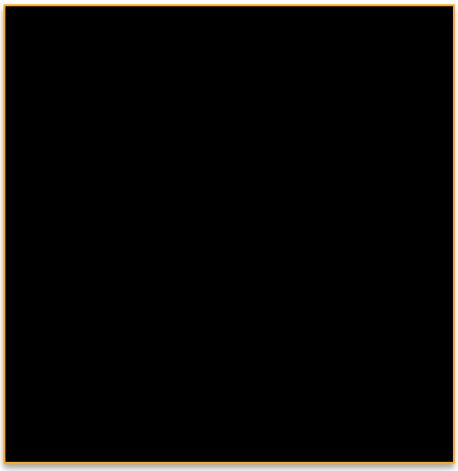

Figure 2 - Moment on Knee Joint From GRF Alignment *[2]*

significantly deviate from a natural stride.

Patients with dorsal flexion weakness will tend to favor load bearing with their toes [1]. The resulting GRF will be located ahead of the knee and the COM, and therefore must be counteracted by excess extension of the knee. This can lead to hyperextension, which means an over stabilized system of bone linkages that can only be destabilized by added force to produce a counteracting moment. This will subtract from the amount of muscle force being applied to propulsion. This lack of propulsive force contribution

provided by the plantar flexors is problematic because it means that regular activities such as walking will become more awkward as there is an imbalance between the pattern of motion the left and right legs are able to create. It can also mean that climbing stairs can become difficult since it requires a minimum amount of propulsion to place the foot at each successive step location. A well-designed AFO should attempt to combat these issues through a combination of variable rigidity and flexibility.

1.2 Problem Statement

Anderson Orthopedics requires an AFO design that can aid in propulsion, compensate for the foot's inhibited dorsal flexion, and aid with plantar flexion weakness (known colloquially as "drop-foot"). This weakness, in addition to contributing to propulsion, can also lead to an increased tendency to trip. Anderson Orthopedics currently produces a variety of AFO designs, however, their existing manufacturing method is overly time consuming and laborious.

Anderson Orthopedics had previously sought the help of a team of students in 2016 to initiate this project, and now wishes to continue progress where the previous iteration left off. The design work thus far has produced a product composed of PC-ISO, chosen for a combination of its elasticity and strength properties that the previous team deemed appropriate for the load conditions of the patient, and for its ability to be 3D printed. The 2016 design lacked quantitative results and data driven decision-making, which has been heavily emphasized in this iteration of the project. The previous team provided a solid foundation, and their achievement will allow our team to focus our efforts and control our scope. With over one month remaining, and an allotted budget of $1000, our team will use the information provided from last year's report to design and quantify an AFO that addresses the needs of Anderson Orthopedics.

1.3 Project Objectives

The objective of the project is to create a quantifiable AFO model and prototype that maximize forward propulsion.

The overall expectations of the team are as follows:

- Provide the patient with a functioning AFO prototype
    - Coordinate manufacturing of AFO prototype
    - Ensure the prototype does not replicate any patented designs
- Perform material testing
- Provide Anderson Orthopedics with the prototype CAD files
- Justify design with quantitative test results
- Justify design with analytical calculations
- Create a process that can be easily adjusted for other patients

2 DESIGN PROCEDURE OVERVIEW

The following section elaborates upon our preliminary, conceptual and final design phases. An in-depth explanation of the optimization phase is given in the Details of Design section. A high-level overview of the design process is detailed in *TABLE I*.

TABLE I: COMPLETE DESIGN PROCESS

Phase	Step	Process
Preliminary Design Phase	1	Establish customer needs, constraints and target specifications.
	2	Evaluate the patient's condition and gather motion capture data.
Conceptual Design Phase	3	Decompose design criteria of AFOs and brainstorm conceptual designs.
	4	Narrow down conceptual designs and select final concepts using weighted matrices.
Pre-Optimization Phase	5	Perform kinematic and dynamic analysis using patient test data.
	6	Determine safety factor and conduct FMEA and fatigue analyses.
	7	Create list of best possible materials to be analyzed during optimization and make a DFAM plan.
	8	Generate concept models based on patient's leg scan in Vorum CANFIT.

	19	Simplify STL files and reduce number of tessellations in Geomagic for SolidWorks.
Optimization Phase	10	Perform meshing, FEA and topology optimization in Altair Hyperworks.
	11	Smooth out optimized result and modify surface geometry in Autodesk Meshmixer.
	12	Re-analyse FEA of modified geometry in Altair Hyperworks.
Final Design Phase	13	Create a solid body, determine the overall specs and create final renders in SolidWorks or CATIA.

2.1 Customer Needs, Constraints and Metrics

The team met with the client and solidified the project needs. Six main categories of needs were identified and further broken into sub-needs. The categories were: (i) AFO is safe, (ii) AFO is easily manufacturable, (iii) Patient needs, (iv) AFO is comfortable, (v) AFO is functional, and (vi) AFO is durable. In total, 35 needs were established. Although all 35 needs were important, some were more critical than others. Prioritizing needs was necessary in order to create a prototype that focused on the fundamental design factors, while still addressing less vital characteristics. The relative importance of needs, or weight, was decided as a team based on the points the client emphasized most in our meeting. See Appendix A1.1 for the complete list of needs. Project constraints were identified in addition to needs. The project was constrained by time, cost, design life, environmental conditions, patient weight, manufacturing method, foot geometry, sensitive areas in the leg, AFO application and removal, and modeling software. Details on these constraints and their limiting parameters are provided in Appendix A1.2.

2.2 Patient Testing and Data Collection

The test patient suffers from Charcot-Marie-Tooth disease (CMT), which is one of North American's most common inherited neurological disorders. CMT affects both motor and sensory nerves, which can limit a person's ability to walk, speak, swallow, and even

breathe. Our test patient noticed a decline in the responsiveness of his left leg just over three years ago. Similar to most CMT patients, the test patient frequently experiences drop foot due to the degradation of the muscles in his lower leg and ankle. Our patient is 74 years old and relatively active. He is currently fitted with a carbon fiber AFO, which is secured by two Velcro straps at the top and middle of the brace. The patient has expressed that he finds the carbon fiber AFO very stiff, making it difficult to walk up and down stairs, and the brace must be removed when he exercises on the elliptical. He also finds the strut uncomfortable on his shin, and had to modify the strut by cutting away some material to leave more room for his tibia. He found the posterior strut from the 2016 model more comfortable than his carbon fiber AFO, but there were some issues with shoe fitment. The team attempted to consider patient preference regarding the stiffness, strut location, and shoe fit while designing our AFO.

2.2.1 Motion Capture

Recording the patient with and without an AFO allowed for gait analysis and the ability to visually quantify how much the device improved the patient's gait. Motion-capture provided information on stride length, walking speed, and relative joint angles. The data points were also used to determine the joint reaction forces and moments on the MTP, ankle, knee and hip.

The patient was marked with twelve bright green stickers, which contrasted his black long underwear. The markers were placed on his heel, MTP, middle toe, ankle, knee and hip on both sides of his body as seen in the image below.

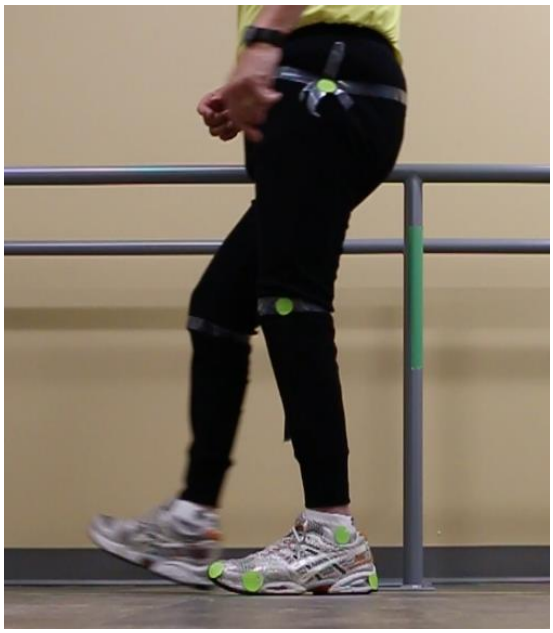

Figure 3: Motion capture markers

Two videos were taken. The patient walked back and forth three times with and without the AFO in the first and second video, respectively. The camera was placed on the floor in the same location for both videos. A foot-long piece of green tape gave a scaling factor for post-processing as seen in Figure *3*.

Post processing was done in Adobe® After Effects™. All six markers were tracked throughout each frame. The raw data was imported into Excel as the video frame number, x location in pixels, and y location in pixels. The units were then converted into standard units of measurement of seconds and mm. The individual frames were first converted to units of time. The motion capture video was shot in 60 FPS, so the equation for the conversion from frames to seconds is as follows:

$$t\,[seconds] = \frac{t\,[frames]}{60\,\left[\frac{frames}{second}\right]}$$

Next, the pixels were converted to relative locations by measuring the number of pixels between two points in the video of known control distance to calculate the meter-pixel conversion factor. The calculation for converting pixels to meters is as follows:

$$x\,[meters] = \frac{x\,[pixels]}{r_{p/f}\,\left[\frac{pixels}{foot}\right]} \times 0.3048\,\left[\frac{meters}{foot}\right]$$

Where $r_{p/f}$ is the ratio of pixels to feet, measured from the control distance. Once all the data points were converted to meaningful units, it was then possible to analyze the data further.

2.2.2 Motion Tracking Data Analysis

The team performed motion tracking on a healthy volunteer to act as a control-case.. This gait dataset was considered to be the “ideal case” and was compared to that of the patient. As mentioned, the patient was tracked with and without an AFO so both data sets were compared to the ideal case.

We isolated eight instances of interest throughout the gait cycle: heel strike, flat foot, mid-stance, contralateral heel strike, heel raise, toe push off, mid-swing and second heel strike. Both heel strikes are necessary to mark the beginning and end of the gait cycle, which provides information of stride length and walking speed. The moment the foot initially lies flat is critical since the ground reaction force is being applied between the heel and the MTP. Mid-stance occurs when the contralateral leg is in mid-swing, and is another interesting point to analyze because the MTP may or may not be subjected to the GRF. The next instant of interest, contralateral heel strike, is arguably the most important. During contralateral heel strike the foot is most effectively transferring GRF load to a vertical acceleration [2]. This is a reasonable metric for gait propulsion. Dividing the moment that occurs at the MTP at the instance of contralateral heel strike by the maximum ankle flexion angle provides a stiffness target for the design. At heel rise, the MTP and toe are still on the ground making it evident that the GRF is travelling at a point between the MTP and toe. Next, toe push off occurs when the MTP has left the ground and only the toe is making contact with the floor. Mid-swing is not an important instant to capture for analysis but we have identified it for graphical benefits. Finally, the second heel strike marks the end of the cycle.

The eight instances were isolated for all three sets of data. *Figure 4* illustrates the relevant frames of the ideal case of a healthy leg without an AFO.

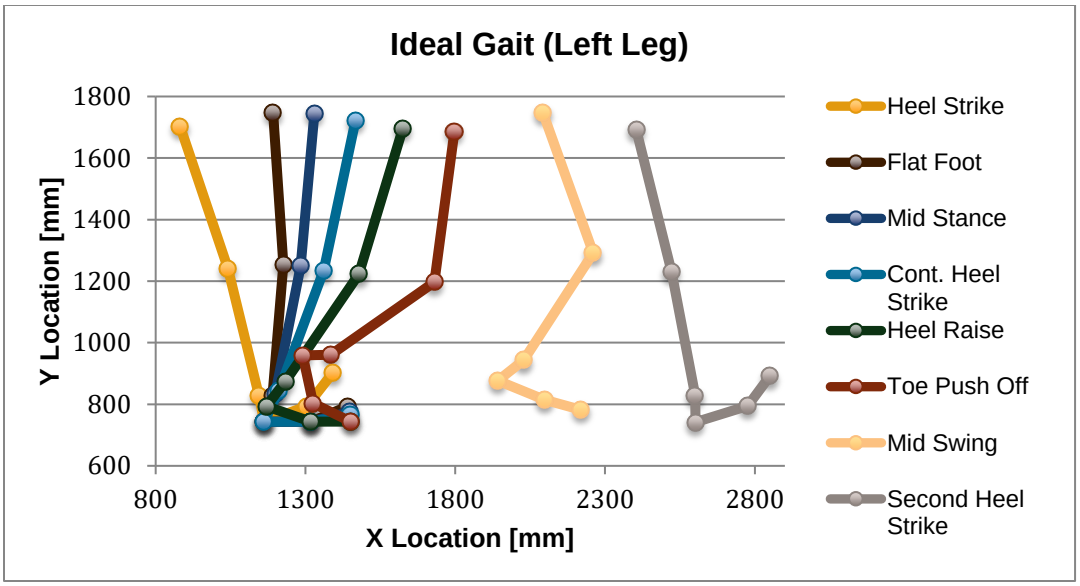

Figure 4: Ideal case healthy leg

As seen in *Figure 4*, the hip moves at a relatively constant rate. There are larger gaps between toe push off and mid-swing, and mid-swing and second heel strike. Another notable characteristic of the ideal gait is the ankle and MTP deflection. The ankle deflection is fairly high at mid swing and second heel strike, respectively. The toes in a healthy gait are able to lift higher and create a smaller ankle flexion angles. Additionally, the MTP deflection at toe push off is very high which provides high propulsion, and a long stride.

As seen in Figure 5, the hip initially moves at a constant rate, but it slows down during heel raise and toe push off. There are also shorter gaps between toe push off and mid-swing, and mid-swing and second heel strike indicating a shorter stride length. The ankle deflection angle is also significantly smaller than in ideal gate. The toes don't lift off the ground as high, also the MTP does not deflect significantly which indicates that the propulsion is lower than the ideal case.

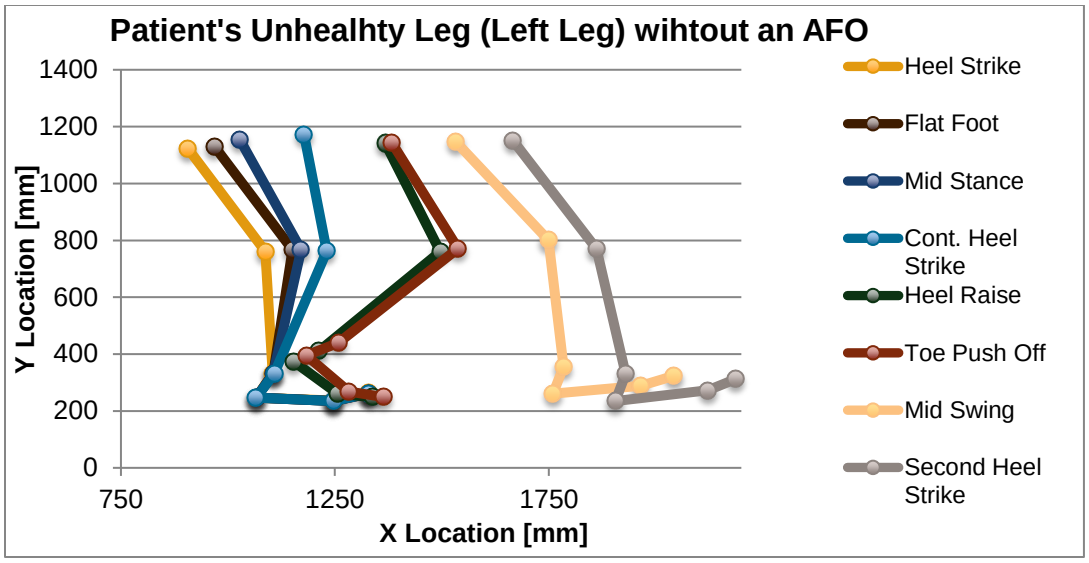

Figure 5: Patient gait cycle without AFO

In Figure 6, a huge improvement in the patient's gait can be observed with the use of the AFO. The hip movement is corrected to move at a constant rate. There are also a increased gaps between toe push off and mid-swing, and mid-swing and second heel strike indicating an increase in stride length. The ankle deflection angle is also improved by the implementation of the AFO. It has a much bigger value than the unhealthy leg data which indicate an improvement in propulsion.

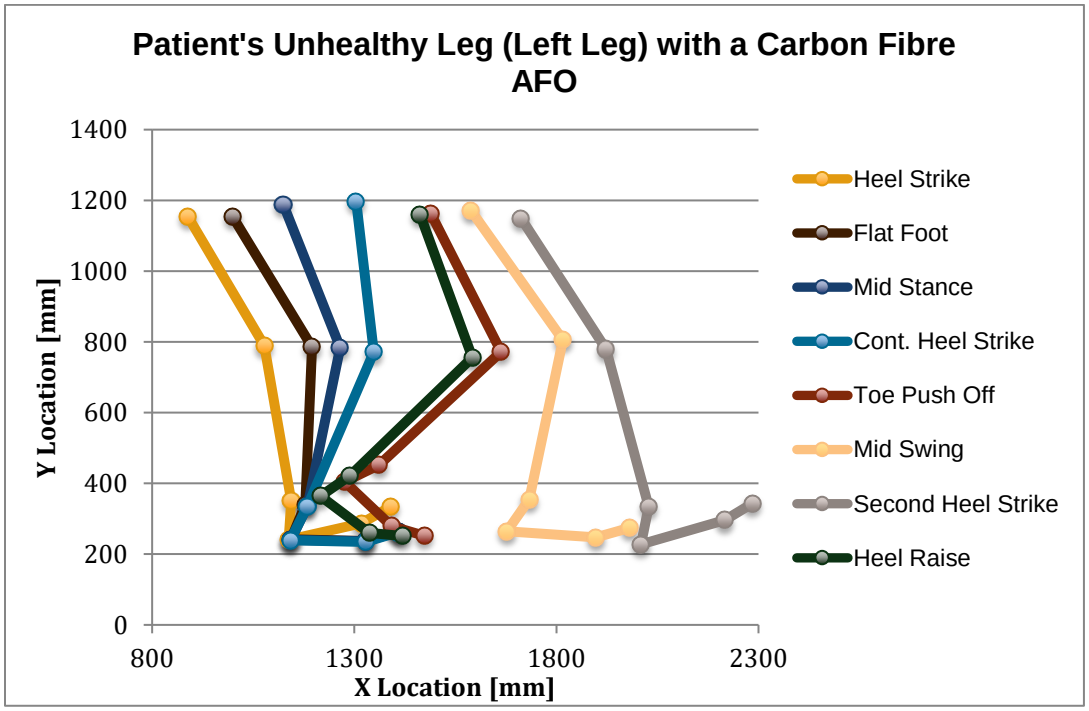

Figure 6: Patient gait cycle with carbon fibre AFO

Subtracting the time difference between the first and second heel strike gives the stride speed in seconds. Similarly, subtracting the heel's X coordinate at second heel strike from first gives the stride length. *TABLE II* summarizes the stride speeds and lengths for all three data sets.

TABLE II: STRIDE SPEED AND LENGTH

	Stride Speed (s)	Stride Length [m]
Patient's Left Leg without AFO	1.55	0.84
Patient's Left Leg with CF AFO	1.42	0.87
Idea Gait Left Leg without AFO	1.10	1.44

As predicted, stride speed and length was slowest and shortest when the patient walks without an AFO. Once the patient was fitted with the carbon AFO, his stride speed decreased by 0.13 s and stride length increased by 30 mm. His stride improved slightly with the brace, but was still nowhere near as fast and long as a healthy gait pattern. The test results of the carbon fiber AFO indicate that the gait of the patient was greatly improved. This implements that our design will also improve the patient's gate to a higher degree.

2.3 PRELIMINARY CONCEPTS

The following section describes the approach for generating AFO concepts to be further analyzed in the detailed design and optimization phases. In total, twenty-one concepts were generated during the initial brainstorming process. From those preliminary concepts, various options for design features were extracted and discussed. Twenty-one concepts were created using information on existing AFOs and general engineering intuition. All designs can be found in Appendix A3.1.

2.3.1 PRELIMINARY CONCEPT DESIGN FEATURES

With patient needs and constraints established and an understanding of the intricacies of human gait and our patient's condition, preliminary concept generation began. Brainstorming lasted several days as the team dissected the benefits and drawbacks of current AFOs on the market. The AFO was broken down into six variables, which include hinge and spring location, hinge and spring symmetry, strut location, heel coverage, lateral support and lastly assembly vs. single component.

Hinge and Spring Location:

The hinge location refers to the location that the AFO is designed to deflect. In the context of this section, the spring force is generated by the deflection of the brace at the hinge location. There were five options for placement of the hinge location on the AFO: Heel, Ankle, Toe (Metatarsal), Heel & Toe, and Ankle & Toe.

Hinge and Spring Symmetry:

Fundamentally, the hinge/spring location on the AFO can either be symmetrical or asymmetrical. In the context of this section, symmetry refers to performance of the hinge, and does not necessarily imply geometric symmetry (since human foot and ankle geometry is not symmetric by nature).

Strut Location:

The strut location refers to the location of the vertical region of the AFO that connects the hinge/spring to the mounting location where the patient loads are applied.

Heel Coverage:

Heel coverage refers to the area of coverage around the heel. There were two design options in this category: partial coverage and full coverage. Partial coverage refers to a design that only contacts the heel at the bottom of the AFO (at the foot plate), leaving a gap in material at the back and sides of the heel. Full heel coverage refers to an enclosed heel design.

Lateral Support:

The cupping of the heel and foot provides the lateral support in an AFO design.

Assembly vs. Single Component:

The assembly design will be made up of two or more components while a single component design will be made up of one part.

2.3.2 PROPULSION POTENTIAL

One of the primary design variables considered during concept selection was the location of the spring. The hinge/spring location dictates what region of the AFO will primarily deflect. At this location, potential energy is stored during the mid-stance phase of gait as the AFO deflects, and energy is released over the course of the terminal stance and pre-stance phases. This process of energy being released provides forward propulsion, which aids the patient in simulating a natural and comfortable walking pattern in the absence of plantarflexion. Providing propulsion was one of the primary functional needs of the AFO, and therefore received a weighting of nine.

Considering a hypothetical AFO, which has a hinge and spring location at the heel, and strut located at the calf. Assuming the hinge component acts as a torsional spring, and that the AFO is fixed to the ground. The case of loading the spring component of the AFO, which is illustrated in Figure 7.

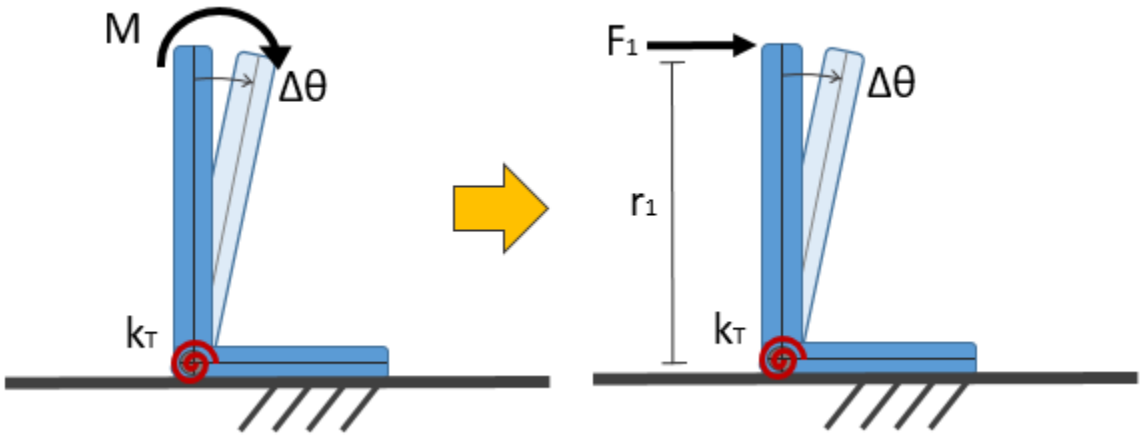

Figure 7: Converting the Applied Moment to a Bending Load at the Top of the AFO Strut

The moment applied to the AFO at the strut can be converted to an equivalent bending load applied at the top of the strut using the following equation:

$$M = F_1\, r_1$$

where r_1 is the perpendicular distance from the applied force F_1 to the hinge location. The spring at the hinge can be approximated as a torsional spring, with spring constant k_t. The spring force is expressed as:

$$M = k_T\, \Delta\theta$$

where Δθ is the angular displacement of the torsional spring. Rearranging the above equation yields:

$$\Delta\theta = \frac{M}{k_T}$$

The equation for maximum stored potential energy in a spring is as follows:

$$PE = \frac{1}{2} k_T (\Delta\theta)^2$$

Substituting equation the equation for theta into the potential energy equation yields:

$$PE = \frac{1}{2} k_T \left(\frac{M}{k_T}\right)^2$$

Furthermore, substituting the moment equation into the new potential energy equation yields:

$$PE = \frac{1}{2} k_T \left(\frac{F_1\, r_1}{k_T}\right)^2$$

Energy is released from the spring as weight is transferred from the AFO foot to the opposite foot during Pre-swing. This situation is illustrated in Figure 8.

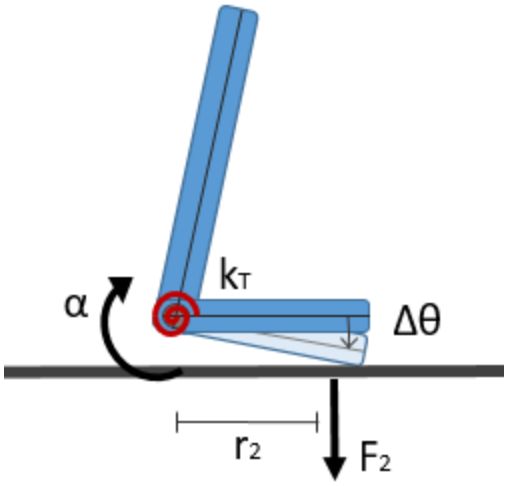

Figure 8: AFO Releasing Potential Energy to Provide Propulsion

The Law of Conservation of Energy states that energy must be conserved in the spring between the two cases of energy storage and energy release. Thus, the following equation, which shows how potential energy was converted from potential to deflect the strut to potential to provide propulsion, holds true:

$$PE = \frac{1}{2} k_T \left(\frac{F_1\, r_1}{k_T}\right)^2 = \frac{1}{2} k_T \left(\frac{F_2\, r_2}{k_T}\right)^2$$

where F_2 is the propulsion force acting between the AFO and the ground, which results in a net angular acceleration of the brace (propelling the using forward), and r_2 is the distance between the AFO spring and the point of application of the propulsion force. Simplifying the above equation yields the following relationship:

$$\frac{F_2}{F_1} = \frac{r_1}{r_2}$$

The relationship shown in the above equation indicates that increasing propulsion force F_2 can be achieved in two ways: (i) by increasing vertical distance from the hinge to the point of application of the AFO load r_1, or by decreasing the horizontal distance from the hinge to the ground reaction force r_2.

Therefore, the optimal hinge location will be that which is as close to the ground reaction force as possible, and as far away from the applied load as possible. Using this statement as criteria for scoring the possible hinge locations, it is clear that placing the

hinge/spring at the toe joint (metatarsal) will provide the best results in terms of propulsion. The analysis used to determine the ideal hinge/spring location is reflected in the results of the concept scoring matrix.

Another possibility for spring locations is to include two separate hinge on the AFO, for example the heel and the toe (metatarsal). While this option would have the benefit of simulating a more natural gait cycle by hinging at both joint locations in the foot, this approach would significantly reduce the overall stiffness of the AFO. Designing for a spring at the heel and toe would result in a system of springs in series, which behave according to the following equation:

$$k_{series,eq} = \frac{k_1 + k_2}{k_1\, k_2}$$

As an example, if the spring constant for both springs was 100N/m, the equivalent spring constant for the system would become 0.02 N/m. The result off adding two spring in series is orders of magnitude less than that of a system with just one single spring of the same stiffness. It is for this reason that including two hinge locations for the AFO was deemed to be undesirable.

On the other hand, having two spring locations parallel to each other will be beneficial, since the spring constant will be added together as shown in the equation below. An example of having two spring in parallel would be having two springs on both sides of the ankle.

$$k_{parallel,eq} = k_1 + k_2$$

Therefore, strictly having the hinge location at the toe is the best option for propulsion potential since it will result in the largest propulsion force.

2.3.3 Design For Patient

The fundamental design process is meant to be repeatable for any patient but individual patients present their own constraints. The patient for this prototype had been exposed to several types of AFOs and very clearly expressed his interest in a posterior strut. The goal was to achieve the best possible propulsion and improve patient gait, however.

Another design consideration is the quality of the patient's other leg. The patient's left leg is primarily affected by CMT but his right leg is also slowly degrading. The AFO could be designed based on the moments in his right leg if it were completely healthy, but it would be unwise to make a device that mimics the behaviour of his right leg since it will gradually worsen. The AFO was therefore designed using the reaction forces and joint moments of a completely healthy gait.

2.4 CONCEPT SELECTION

The twenty-one conceptual designs combined the seven previously mentioned design features differently in the hopes of coming up with the best concept. In general, increasing the number of concepts to select from increases the probability of arriving at the optimal design. A series of concept selection matrices were used to qualitatively score all potential design combinations based on engineering logic and some preliminary analyses for certain critical design features. Rather than restricting choices to the 21 concepts, the selection approach encompassed all of the possible design permutations and systematically ranked them against criteria determined from the customer needs. The six design criteria were then weighted by level of importance to the overall success of the design. Some criteria items are more critical to the design and therefore they will have a higher overall weighting out of ten. This weighting was in some cases subjective, but was largely driven by the needs specified by the client, and by the relevant theory and background information. The weighted design variables are shown in TABLE III.

TABLE III: SUMMARY OF DESIGN VARIABLES TO BE CONSIDERED FOR CONCEPT SCORING

Design Category	**Number of Design Options per Category**	**Category Weight (Out of 10)**
Hinge/Spring Location	5	10
Hinge/Spring Symmetry	2	8
Strut Location	4	7
Heel Coverage	2	4
Lateral Support	3	8
Assembly vs. Component	2	7

One obvious omission to the Design Variable category in TABLE III is Fastening Method, which would describe the design options for fastening the AFO to the patient's leg. Ultimately, the fastening method is outside of the project scope, and can be determined separately and retrofitted into the design at a later date. For the purpose of prototyping, a simple Velcro strap will serve as the fastening method.

Additionally, each of the variables will have multiple options to choose from. Tahe best option will be chosen based on how they score on each of the applicable 16 functionalities that the AFO design must provide as seen in TABLE IV below.

TABLE IV: LIST OF CLIENT NEEDS USED FOR SCORING DESIGN OPTIONS IN THE CONCEPT SELECTION MATRICES

#	**Need #**	**Need Description**
1	N 1.3	Propulsion Potential
2	N 1.2	Simulates Natural Gait Cycle
3	N 3.1	Consequence of Failure
4	N 3.4	AFO Does Note Rub on Skin
5	N 3.5	Avoids Sensitive Areas
6	N4.1 to N 4.4	Ease of Manufacturing
7	N 5.3	Discrete Design
8	N 6.5	Opportunity for Weight Reduction
9	N 6.4	Shoe Fit
10	N/A	Complexity
11	N 1.5	Provides Lateral Stability

Since there were six design categories that influenced the overall conceptual design, six individual decision matrices were created. For each decision matrix, each design option was scored out of four against the needs, and each need was weighted according to its importance within the category using a 9-3-1 weighting scale (9 = Very Important, 3 = Somewhat Important, 1 = Less Important). The 9-3-1 weighting scale was used to

emphasize the most critical needs, ensure that those critical needs have the greatest influence over the design.

Concepts were scored using a rating scale from one to four, with the highest scoring concept being the most advantageous. In general, the highest scoring design option within a category received a score of four, and all other options received proportionately lower scores. The scoring process is based largely on engineering intuition and backed by the research conducted by the team, but there is still an aspect of objectivity that cannot be ignored.

Once all design options were scored for all relevant needs a total was calculated for that design option based on the formula below:

$$T_j = \sum_{i=1}^{m} s_{ij}\, w_i \quad (9)$$

where T_j is the total score for a j^{th} design option, s_{ij} is the j^{th} design option's individual score for the i^{th} need, w_i is the weighting value for the i^{th} need, and m is the total number of needs.

Once all the totals were calculated for each design option, the totals were normalized based on the overall design category weighting. The normalization process ensures that the highest scoring design option within a given category receives full marks for that category (i.e. 100% of the design category weighting value). For example, if the overall weighting value for a particular category was 8.00, the highest scoring design option within that category would end up with a total normalized score of 8.00, and all other design options would receive scores less than 8.00 in proportion to their respective totals. The equation used to normalize the totals for each design option is shown below:

$$N_j = \frac{T_j\, W}{MAXIMUM\{T_1, T_2, \ldots, T_n\}}$$

Where N_j is the normalized score for the j^{th} design option, W is the normalizing value for the design category, and n represents the total number of design options. The layout of the selection matrix scoring design options against customer needs for a particular design category is shown in TABLE V.

TABLE V: EXAMPLE SCORING MATRIX FOR COMPARING DESIGN OPTIONS TO CUSTOMER NEEDS FOR A PARTICULAR DESIGN CATEGORY

	Needs (i) /	i = 1	i = 2	...	i = m	Normalized Total
	Weighting	w_1	w_2	...	w_m	W
Options (j)	j = 1	s_{11}	s_{12}	...	s_{1m}	N_1
	j = 2	s_{21}	s_{22}	...	s_{2m}	N_2
	...	...	...	...	...	...
	j = n	s_{n1}	s_{n2}	...	s_{nm}	N_n

2.5 KINEMATIC AND DYNAMIC ANALYSIS

The converted data points were analyzed in Microsoft Excel in order to acquire quantitative data about the patient's gait kinematics. The objectives for analyzing the motion capture data were:

- Determine joint locations over the course of the entire gait cycle for each area of interest. This was achieved by plotting the x and y coordinates for the hip joint, knee joint, ankle joint, metatarsal joint, heel, and toe tip.
- Determine the motion of joints over time during gait. This was achieved by plotting x coordinates and y coordinates over time for the hip joint, knee joint, ankle joint, metatarsal joint, heel, and toe tip.
- Determine flexion angles during gait. This was achieved by calculating flexion angles and plotting them over time for hip flexion, knee flexion, and ankle flexion.
- Determine the patient's walking speed.
- Determine the patient's stride length.

All of the parameters listed above would be calculated for four cases:

1. No AFO, Unhealthy Leg
2. No AFO, Healthy Leg
3. With AFO, Unhealthy Leg
4. With AFO, Healthy Leg

All of these parameters were then compared to the idealized patient model to recognize discrepancies. The idealized model was a healthy gait cycle that was scaled to the patient's measurements. Scaling the ideal data set minimized inconsistencies in the while comparing. These discrepancies became the design targets. The results from this analysis were also used to validate the final design.

Next, we determined the linkage lengths using the following equation:

$$\left|\left|\vec{u}\right|\right| = \sqrt{(x_2 - x_1)^2 + (y_2 - y_1)^2}$$

Using the following equation, the unit vectors for the ground plane, GRF line of action, femur, tibia, foot, and toe were calculated.

$$\vec{u} = \begin{bmatrix} (x_2 - x_1)/\left|\left|\vec{u}\right|\right| \\ (y_2 - y_1)/\left|\left|\vec{u}\right|\right| \end{bmatrix}$$

The angle between two vectors ***u*** and ***v*** is as follows, which was used to determine flexion angles:

$$\theta = \cos^{-1}\frac{(\vec{u}\cdot\vec{v})}{\left|\left|\vec{u}\right|\right|\cdot\left|\left|\vec{v}\right|\right|}$$

The flexion angular velocities and flexion angular accelerations were calculated using the following two equations:

$$\dot{\theta} = \frac{d\theta}{dt} = \frac{\theta_2 - \theta_1}{t_2 - t_1}$$

And

$$\ddot{\theta} = \frac{d^2\theta}{dt^2} = \frac{d\dot{\theta}}{dt} = \frac{\dot{\theta}_2 - \dot{\theta}_1}{t_2 - t_1}$$

In order to consider the rotational inertia of each linkage individually, it was necessary to convert the flexural angular accelerations to a local-linkage coordinate system.

$$\alpha_{foot} = \dot{\theta}_{ankle} - \alpha_{tibia}$$

$$\alpha_{tibia} = \dot{\theta}_{knee} - \alpha_{femur}$$

$$\alpha_{femur} = \dot{\theta}_{hip}$$

From NASA documents, values for relative body segment weights, center of mass locations, and mass moment of inertia (MMOI) values can be determined.
Estimating body segment weights [1]

$$m_{foot} = 0.0069\, m_{total} + 1.04\ [lbm]$$

$$m_{shank} = 0.0375\, m_{total} + 0.84\ [lbm]$$

$$m_{thigh} = 0.1159\, m_{total} - 2.25\ [lbm]$$

Body segment center of mass locations can be expressed as a percentage of total segment length:

Table VI: Approximate body segment center of mass locations as a percentage of total segment length [1].

Segment	**Location [% of Total Length]**	**Reference Point**
Thigh	41%	Hip Joint
Shank	44%	Knee Joint
Foot	44%	Heel

Body segment mass moments of inertia are needed to calculate total rotational inertia of each segment.

Table VII: Approximate MMOI values for body segments [NASA].

Segment	**MMOI [kg/m^2]**
Thigh	6.734
Shank	6.397
Foot	0.488

2.5.1 GRF DATA

The patient's ground reaction force magnitude in the vertical direction is an important starting point for solving the system of interacting dynamic loads in the patient's leg, and is therefore important to assess with some level of precision. The method used to collect this data involved a brief test whereby a balance board with 4 strain gages at each corner was placed on a floor space, and the patient was asked to walk over the plate. The strain gages deflect in small amounts and vary in resistance based on these measurable values. Corresponding to the change in resistance, the gages output a varying voltage dependent on the magnitude of the deflection. These values can be constantly sampled while the balance board is turned on, however, they require a data acquisition method to determine the sampling and store the information. In addition, the averaged center of pressure (COPX, COPY), can be directly derived from individual

gage readings, and is calculated by the following equation:

$$COP_x = \frac{L}{2}\frac{((TR + BR) - (TL + BL)}{(TR + BR + TL + BL)}$$

Where TR, BR, TL, BL are the readout values from each individual strain gage, and L is the distance in the X-direction between gages.

The GRF recording tests were conducted such that the observed gait patterns were natural and noticeable

The signal transmitted from the board is converted from an analogous value to discretely sampled data points with a varying frequency dictated by behavior of the Bluetooth connection between the board and connected laptop.

Under the assumption that there is no net acceleration of the patient's center of mass (which was deemed valid because the patient exhibited near constant walking speed and no average net acceleration of the hip joint), then the GRF line of action can be determined by drawing a line from the point of application of the GRF to the body's center of mass. Using Pythagorean Theorem, the horizontal component can be determined as follows:

$$GRF_x = \frac{GRF_y}{\tan\varphi}$$

Where φ is the angle between the GRF line of action and the vertical plane.
The next step was to determine the joint reaction moments based on the Free-Body analysis of each individual segment (foot, toe, tibia, femur). This was done under three cases:

1. Stance Phase, GRF applied behind the MTP (meaning no load applied to toe linkage)
2. Stance Phase, GRF applied ahead of the MTP (meaning the MTP joint is loaded by the GRF)
3. Swing Phase (only body segment weights contribute to joint reaction moments).

Joint reaction moments were used as a comparison metric for determining if the “before” and “after” case to see if the AFO was truly successful in reducing the patient’s overall joint effort and contributing to propulsion. Joint reaction moments can be determined from the experimental motion capture data since all of the linkage accelerations are known, along with the patient’s approximate COM information and GRF data (external forces).

Below is a full analysis of the dynamics in each case.

Dynamics

The dynamics analysis was based on Newton’s second law, which is represented in two dimensions by the following three equations:

$$\sum F_x = m\, a_x$$

$$\sum F_x = m\, a_y$$

And

$$\sum M = I\, \alpha$$

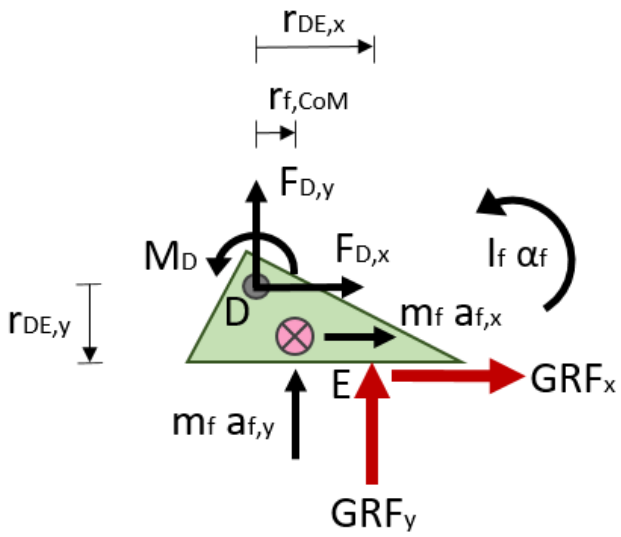

Figure 9: Foot FBD

Based on Newton’s second law, the joint reaction forces and moments can be determined for the foot. When the centre of pressure of the GRF landed between the heel and the MTP, the following equations were used:

$$F_{D,x} = m_f\ a_{f,x} - F_{GRF,x}$$
$$F_{D,y} = m_f\ a_{f,y} + m_f\ g - F_{GRF,y}$$
$$M_D = I_f\ \alpha_f + m_f\ g\ r_{f,COM} - F_{GRF,y}\ r_{DE,x} - F_{GRF,x}\ r_{DE,y}$$

Conversely, we applied the next three equations when the GRF between the MTP and the heel.

$$F_{D,x} = m_f\ a_{f,x} - F_{MTP,x}$$
$$F_{D,y} = m_f\ a_{f,y} + m_f\ g - F_{MTP,y}$$
$$M_D = I_f\ \alpha_f + m_f\ g\ r_{f,\square OM} - M_{MTP,y} - F_{MTP,y}\ r_{DE,x} - F_{MTP,x}\ r_{GRF,y}$$

Next we considered the reactions at the tibia. A free body diagram of the tibia is seen in *Figure 10*.

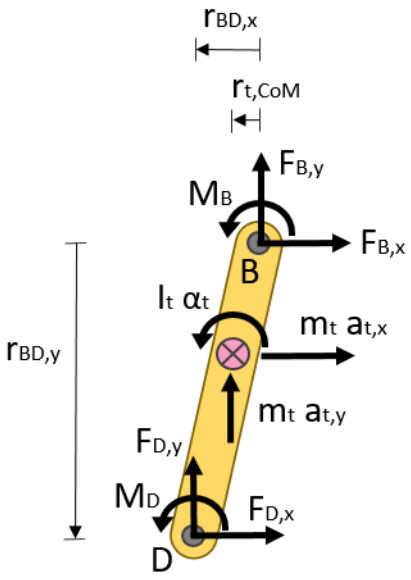

Figure 10: Tibia FBD

The reaction forces and moments on the tibia were determined as follows:

$$F_{B,x} = m_t\ a_{t,x} - F_{D,x}$$
$$F_{B,y} = m_t\ a_{t,y} + m_t\ g - F_{D,y}$$
$$M_B = I_t\ \alpha_t - m_t\ g\ r_{t,COM} - M_D - F_{D,x}\ r_{BD,y} + F_{D,y}\ r_{BD,x}$$

Finally, *Figure 11* depicts the forces and moments on the femur.

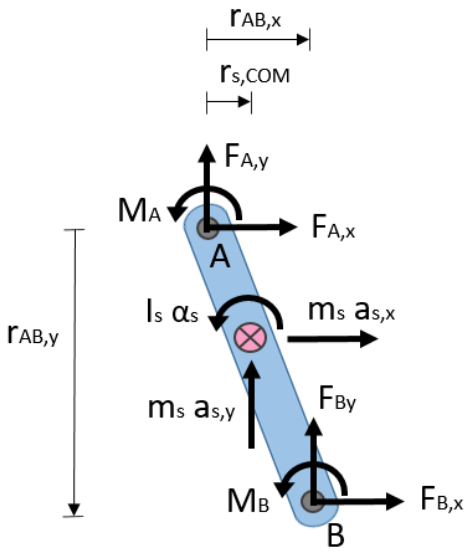

Figure 11: Femur FBD

Similar to the tibia equations, forces and moments were calculated using the equations below:

$$F_{A,x} = m_s\, a_{s,x} - F_{B,x}$$

$$F_{A,y} = m_s\, a_{s,y} + m_s\, g - F_{B,y}$$

$$M_B = I_s\, \alpha_s + m_s\, g\, r_{s,COM} - M_B - F_{B,x}\, r_{AB,y} - F_{B,y}\, r_{AB,x}$$

Full joint reaction moment analysis was performed with data sets from patient testing as well as the scaled idealized gait. See appendix A for the final results of all three data sets.

The optimal stiffness is obtained from the maximum possible deflection at the instance of contralateral heel strike [2]. In order to determine the maximum amount of MTP flexion that can be achieved without causing irregular/uncomfortable gait, we used the pendulum approximation. This approximation allows us to keep knee flexion constant during stance phase while the toe and MTP are pinned and only the heel is able to lift off the ground plane. Figure 13 depicts the model as the foot sits flat on the ground while Figure 13 shows the raised heel, pinned toes, and forward hip.

Figure 12: Flat foot pendulum approximation

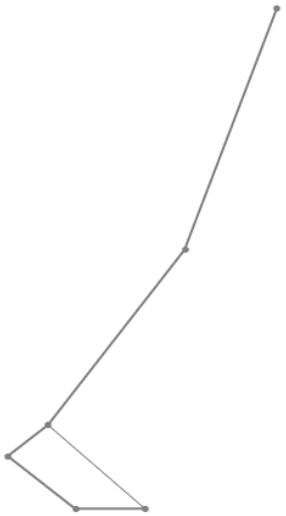

Figure 13: Heel raise pendulum approximation

The ankle flexion angle of the scaled idealized model at contralateral heel strike was used as the target angle in the pendulum model. Data points were gathered at all six locations once the model was adjusted to the target angle. Three sets of data points were taken at varying angles leading up to optimal angle. This data set was then run through the kinematics and dynamic spreadsheet to determine the joint reaction forces and moments.

The target stiffness is related to the optimal flexion angle and moment at the MTP as follows:

$$M = k_t \vartheta$$

Based on the scaled ideal results, the moment at the MTP at contralateral heel strike was 38.6 N-m and the ankle flexion angle was 150.6°. Therefore the maximum stiffness value was determined:

$$k_t = \left(\frac{M_{MTP}}{\vartheta_{ankle}}\right)$$

$$k_t = \left(\frac{38.6}{180-150.6}\right) = 1.31 \text{ N-m/°}$$

The linear stiffness was calculated from the torsional stiffness as follows:

$$k_l = \left(\frac{k_t}{r_{afo}}\right)\left(\frac{180}{\pi}\right)$$

$$k_l = \left(\frac{1.31}{0.381}\right)\left(\frac{180}{\pi}\right) = 517.2 \text{ N/m}$$

Both stiffness and load cases are required for Hyperworks optimization, but the free body diagrams and equations displayed thus far do not account for an AFO. Introducing a brace into the system causes the patient's foot, ankle, and tibia to behave as a rigid member, affecting the overall reaction forces and moment equations. The AFO applies a force (F_{afo}) at the fastening location. As previously mentioned, load cases at the instances of initial heel strike, initial flat footedness, mid-stance, contralateral heel strike, heel raise, toe push off, mid-swing and second heel strike are critical. These eight frames were isolated and their load cases were determined in the X direction. We did not consider loads in the Y direction since the footplate takes them and they do not contribute to deflection.

The $F_{afo,x}$ values were determined using a series of equations. Distance afo_x was calculated first. The height of the AFO was divided by the knee height, multiplied by the difference in X values of the knee and ankle added to the ankle X value. The equation is shown below:

$$afo_x = \left(\frac{afo_y}{r_k}\right)(x_{knee} - x_{ankle}) + x_{ankle}$$

The distance afo_y was calculated in a similar fashion:

$$afo_y = \left(\frac{afo_y}{r_k}\right)(y_{knee} - y_{ankle}) + y_{ankle}$$

Next, the distance from the AFO to the MTP was calculated:

$$afo_{tot} = (\left(\sqrt{((afo_x - MTP_x)^2 + (afo_y - MTP_y)^2)}\right))/1000/1000$$

Finally, dividing the moment produced at the MTP by the total distance yields the applied force in the X:

$$F_{afo,x} = \left(\frac{M_{MTP}}{afo_{tot}}\right)$$

The $F_{afo,x}$ values were plugged into Hyperworks to simulate the device loading.

2.6 SAFETY FACTOR, FMEA AND FATIGUE ANALYSES

The FMEA was done for the AFO as it goes through the different stages of the gate cycle. The heel raise/ toe push off process was the most critical since it had the highest number of failure modes and the highest RPN value of 243 for the fatigue failure at hinge mode. Other concerning modes were; brittle fracture at the lower strut or the footplate at the hinge location which, both had an RPN of 216. The least concerning processes were; the flat foot and the swing phase which, both had no potential failure modes. More details can be seen in the table below.

TABLE VIII: FMEA FORM [3]

Process Step /Input	Potential Failure Mode	Potential Effect	SEV	Potential Causes	FREQ	Current Controls	DET	RPN	Actions Recommended
Heel Strike	Foot plate fractures near heel region	Injure patient's heel	9	Large load on heel part of foot plate as the heel strikes the ground	1	Training: learning the AFO's limitations (no jump off of platforms, no kicking objects with AFO foot, no walking on uneven terrain, etc.)	8	72	-Follow the AFO training instructions
Heel Strike	Lower part of strut fractures	Injure patient's ankle	9	Large asymmetric load on heel as it strikes the ground(stepping on a pebble)	3	Training: learning the AFO's limitations (no jump off of platforms, no kicking objects with AFO foot, no walking on uneven terrain, etc.)	8	216	-Follow the AFO training instructions -Use best judgement to not over strain the AFO
Heel Strike	Lower part of the strut	Strut will contact	3	Large asymmetric	3	Training: learning the AFO's limitations	8	72	-Follow the AFO training instructions

Process Step /Input	Potential Failure Mode	Potential Effect	SEV	Potential Causes	FREQ	Current Controls	DET	RPN	Actions Recommended
	buckles inward (bends in unwanted direction)	patient's ankle causing discomfort		load on heel as it strikes the ground(stepping on a pebble)		(no jump off of platforms, no kicking objects with AFO foot, no walking on uneven terrain, etc.)			-Use best judgement to not over strain the AFO
Flat foot	none	---------	-	------	-	------	-	-	------
Heel raise/ Toe push off	Lower part of strut fractures	Injure patient's ankle	9	-Excessive bending angles on the AFO -Excessive torsion angles on the AFO	3	Training: learning the AFO's limitations (no jump off of platforms, no kicking objects with AFO foot, no walking on uneven terrain, etc.)	8	216	-Follow the AFO training instructions -use best judgement to not over strain the AFO
Heel raise/ Toe push off	Lower part of the strut buckles inward (bends in unwanted direction)	Strut will contact patient's ankle causing discomfort	3	-Excessive bending angles on the AFO -Combination of excessive torsional and bending of the AFO	3	Training: learning the AFO's limitations (no jump off of platforms, no kicking objects with AFO foot, no walking on uneven terrain, etc.)	8	72	-Follow the AFO training instructions -Use best judgement to not over strain the AFO
Heel raise/ Toe push off	Foot plate fracture at hinge	Injure patient's MTP	9	-Excessive bending angles on the AFO	3	Training: learning the AFO's limitations (no jump off of platforms, no kicking objects with AFO foot, no walking on uneven terrain, etc.)	8	216	-Follow the AFO training instructions -Use best judgement to not over strain the AFO
Heel raise/ Toe push off	Fatigue failure at hinge	Injure patient's MTP	9	Excessive bending angles on the AFO	3	-Checking for cracking and other signs of fatigue failure. -Training: learning the AFO's limitations (no jump off of platforms, no kicking objects with AFO foot, no walking on uneven terrain, etc.)	9	243	-Follow the AFO training instructions -Use best judgement to not over strain the AFO -Replace AFO every two years

Process Step /Input	Potential Failure Mode	Potential Effect	S E V	Potential Causes	F R E Q	Current Controls	D E T	RPN	Actions Recommended
Swing	none	------	-	------	-	------	-	-	------

The overall factor of safety is determined by five main values, which are the material, stress, geometry, failure analysis and reliability factors of safety. All these factors of safety can be multiplied together to determine the overall factor, as shown in the equation below. [4]

$$FS = FS_{material} * FS_{stress} * FS_{geometry} * FS_{failure\ analysis} * FS_{reliability}$$

The material factor of safety can range from 1.0 to 1.4. If the material properties are well known, we can assign a factor of safety of 1.0 and if they are not well defined, a safety factor of 1.4 will be used. [4].

For this project, the material properties are not very well known therefore, a safety factor of 1.4 was used as shown below.

$$FS_{material} = 1.4$$

The load factor of safety can range from 1.0 to 1.7. If the load cases are well known, we can assign a factor of safety of 1.0 and if they are not well defined, a safety factor of 1.7 will be used. [4]

The load cases are well defined for regular gate, but there can still be load cases that were not accounted for. Therefore, a factor of safety of 1.5 will be assigned as shown below.

$$FS_{stress} = 1.5$$

The geometry safety factor has a range from 1.0 to 1.2. If the manufacturing tolerances are very tight the factor of safety will be 1.0. On the other hand, if the dimensions are not closely held to the CAD model, then a safety factor of 1.2 will be used. [4]. The geometry tolerance will be average and therefore, a safety factor of 1.0 will be used.

$$FS_{geometry} = 1.0$$

If the failure analysis to be used is derived for the state of stress or fatigue stresses and is a well-developed failure analysis, then a factor of safety of 1.0 will be assigned. If the failure analysis in not well developed then a factor of safety of 1.5 will be used. [4]
Since the failure analysis is well developed for this project, a safety factor of 1.0 is used, as shown below.

$$FS_{failure\ analysis} = 1.0$$

If the reliability does not need to be high then a factor of safety of 1.1 will be used. If a reliability of 92%-98% is needed then a safety factor of 1.2-1.3 will be used. For a 99% reliability use safety factor of 1.4-1.6. [4]
This design needs a moderate reliability and therefore, a factor of safety of 1.2 will be used.

$$FS_{reliability} = 1.2$$

Since all the variables were determined for equation, the overall safety factor was be determined to be 2.52,as shown below.

$$FS = 1.4 * 1.5 * 1.0 * 1.0 * 1.2$$
$$FS = 2.52$$

Fatigue analysis is a critical failure mode for this design, since the AFO will be undergoing numerous load cycles. The ankle-foot brace needs to last the patient for a full two years, which translates to 5,000,000 load cycles without failing. The equation below will be used to determine the maximum fatigue stress, where S_n is the total fatigue stress, S_n' is the theoretical fatigue stress, and the modifying factors which are; C_M the material factor, C_{st} is the stress factor, C_r is the reliability factor and C_S is the geometry factor [5]

$$S_n = S_n{}' C_M C_{st} C_r C_g$$

The theoretical fatigue stress is determined to be 6.5 MPa from the S-N curve below, given that the number of cycles is 5,000,000.

The S-N curve shown below is for PLA, which is not the material that will be used for the AFO design, but it gives a general idea of what the fatigue failure study looks like.

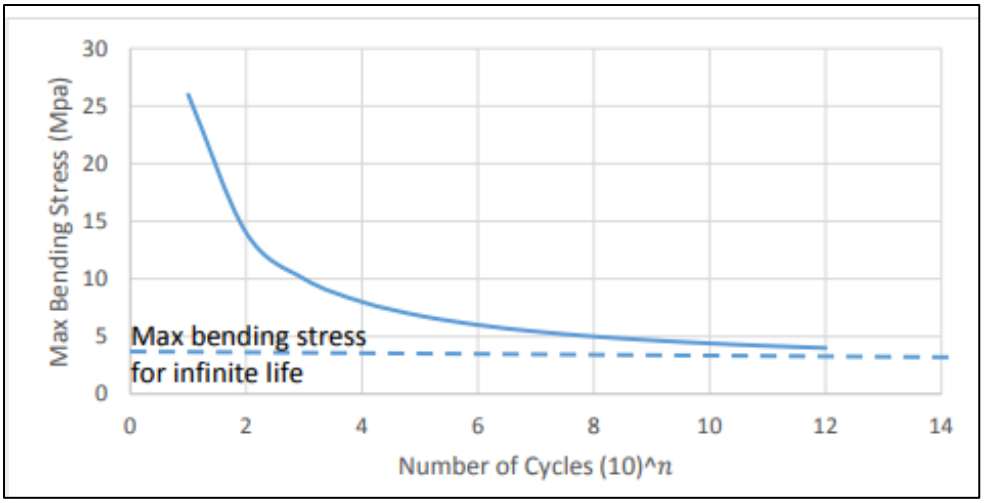

Figure 14:PLA maximum bending stress Vs. number of cycles [6]

The modifying factors C_M, ,C_{st} ,C_r ,C_g were determined to be 0.71, 0.66, 0.83 and 1.0. These factors are the inverse of the factor of safety in section.

The total fatigue stress for the AFO design cannot exceed 2.53Mpa, as derived below.

$$S_n = 6.5 * 0.71 * 0.66 * 0.83 * 1.0$$

$$S_n = 2.53Mpa$$

2.7 MANUFACTURING METHODOLOGY AND DFAM

The considerations for the manufacturing of this AFO include an emphasis on pushing the device's design space to the level of complexity the freedom of 3D printing methods

allow. Indeed, geometric freedom is quite increased over most traditional machining methods, but AM approaches do still have their own set of unique constraints.

2.7.1 MANUFACTURING METHODOLOGY

Pursuing a 3D printable design required an atypical approach to manufacturing considerations. The design approach took into consideration 3 prominent AM methods: SLS, FDM and Stereolithography. Decisions for determining the appropriate material choice were reassessed so as to keep several mechanically advantageous options in consideration. A comparison of each method was necessary to determine how to best take advantage of the AM geometry freedom. The initial scoring of each respective method is detailed in APPENDIX B.

The team chose filament deposition modelling (FDM) as the appropriate manufacturing method for the device. This method was ideal because it allowed for short lead time, which was a necessity for producing an initial prototype. There are tradeoffs to every method of additive manufacturing, and FDM is no exception. The considerations for which method to use were left up to the team, so several relevant factors needed to be considered in making this choice.

FDM, like most methods of AM, revolves around layering of heated material that is, upon cure, weak in the transverse direction. FDM filament parts exhibit what is known as a raster angle, which is the relative angle between the filament layering plane and the direction of loading. FDM, compared to SLS and STL, exhibits the biggest knockdown in mechanical strength when loading out of plane from the raster angle. This, in addition with the fact that suppliers do not provide thorough knockdown info in their material specifications, makes for an added challenge in properly analyzing a part's failure modes. To circumvent this data gap, the assumption was made that the absolute worst-case conditions for the stiffness characteristics, as per specification data, would be used to optimize the stiffness characteristics of the geometry. The guarantee with this assumption is that

In addition to anisotropy due to rasterization, FDM filaments tend to be brittle with low strain to failure and low tensile properties. Ideal mechanical properties were considered to be those in materials that exhibited an optimal combination of maximum strain energy

storage in bending.

Maximizing this storage capacity, as well as adequate stiffness such that the device would mitigate drop foot behavior.

Quotes for materials that exhibited ideal strain energy storage characteristics were sourced, which made it immediately clear how confined the material options would be. Using the 2016 prototype to obtain comparative pricing, it was made clear that SLS methods were universally not realistic within budget. The strain energy, elongation to break and associated cost of each material was compared to produce several pursuable options for FEA optimization analysis.

Following the time constraints of the project schedule, priority was shifted towards manufacturing methods with low lead time. This would eventually make Precision ADM the optimal choice for lead time along with print bed size, as they are the only printing company in Manitoba equipped with the large-scale Fortus 900mc.

The options above reference various quotes generated from the 2016 model as received from the manufacturing sources considered.

Table 9 - AM MATERIAL DATA

Material Choice	Method	Tensile Strength* (Mpa)	Tensile Modulus (Mpa)	Elongation at Break	Density	Quote (If Obtained)	Source
Windform XT	SLS	83.43	8928.2	3.8	1.097		
Windform SP	SLS	76.1	6219.6	11.38	1.106		
Windform FX	SLS	50.74	1908	50.3	1.022		
Windform GT	SLS	56.21	3289.8	14.82	1.19	3000 USD	CRP
Windform GF	SLS	50.6	4304	4.6	1.41		
Alumide	STL	48	3800	4	1.36	318 EUR	Materialise
Proprietary CF Nylon	FDM	63.9	4387	4	1.14	200 USD	3DXTech
CF PETG	FDM	55.5	4928	2.5	1.34		
CF PLA	FDM	47.9	4791	2	1.29		
CF ABS	FDM	44	4018	1.8	1.11		
TuskXC2700T	STL	53.6	2880	20	1.18	328 EUR	Materialise
PerForm	STL	78	10500	1.1	1.61		

PC ISO	FDM	57	2000	**4**	Not listed	885 CAD	Heartland
Nylon 12 GF	SLS	36	2896	3	1.25	1200 USD	Stratasys
Polyamide GF	SLS	51	3200	6	1.22	253 EUR	Materialise
Ultem 9085	FDM	33	2270	1.7	1.34	1030 CAD / 679 EUR	Heartland / Materialise
Ultem 1010	FDM	37	2200	1.5	1.27	975 CAD / 1542 CAD	Heartland / Cimetrix
* Z-Axis Properties Listed if Anisotropic Properties Given							

[7] [8] [9] [10] [11]

Notably, there was not an observed trend between material properties and quoted cost to print, but rather the cost to print was very dependent on the provider, and the manufacturing process. In general, SLS materials tended to be more prohibitively expensive. Given their perceived reduction in anisotropy, the cost increase in utilizing SLS materials comes with increased ease of analysis.

Strain energy is a property of strong consideration for a heavily loaded part being used for elastic spring-back. The more strain energy stored, the more propulsive reaction loading can be provided by the AFO without yielding the device. Strain energy is represented by:

$$U = \frac{1}{2}(V * \sigma^2)/E$$

Where V is the volume of the part in question, which would remain constant for comparison, sigma represents the planar stress, and E the planar modulus of the material.

By this metric, the materials scored as follows:

Table 10 - MATERIAL STRAIN ENERGY CAPABILITIES

Material Choice	Max Strain Energy (kJ/cubic meter)	Ranking
Windform XT	389.8078504	8
Windform SP	465.5612901	5
Windform FX	674.6718029	2
Windform GT	480.2061068	4
Windform GF	297.4395911	12
Alumide	303.1578947	11

Proprietary CF Nylon	465.3761112	6
CF PETG	312.5253653	9
CF PLA	239.4500104	16
CF ABS	240.9158785	14
TuskXC2700T	498.7777778	3
PerForm	289.7142857	13
PC ISO	812.25	1
Nylon 12 GF	223.7569061	17
Polyamide GF	406.40625	7
Ultem 9085	239.8678414	15
Ultem 1010	311.1363636	10

With respect to strain energy as the only metric, the FDM-printable material PC ISO, which was used in the previous prototype, is evidently the most optimal choice.

Given that the optimization process dealt with limited design space and therefore an imposed limitation on maximum achievable stiffness variation through geometry modification, a material could not easily be narrowed down until optimization had yielded results to indicate that the final design could achieve the performance-preferred deflection under the patient's load case. Therefore, multiple materials were analyzed.

2.7.2 Design For Additive Manufacturing

Designing for an additive approach requires a modified approach for manufacturability. Whether utilizing resin curing, powder bed fusion or fused filaments, the process of manufacturing involves the layer by layer curing of heated material. Therefore, while geometric freedom in design is increased, it is not perfect freedom.

A main consideration for DFAM is optimization of various project parameters for cost reduction. Cost optimization is inherent in the mass reducing approach of topology optimization, but an excess of overhang angles in a design can create an increased necessity of support structure inclusion. Overhangs are free edges on the bottom of a part's geometry. Because the layering process of most AM methods would not allow for the material to properly cure without more material at its base, the result of unsupported overhangs will be a severely compromised surface finish with dubious effect on mechanical properties.

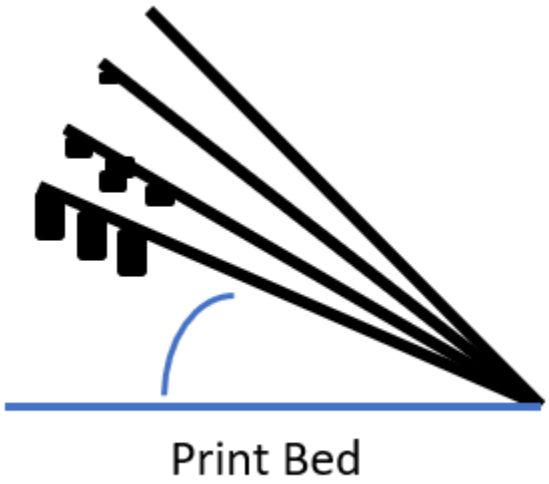

Figure 15: Print bed orientation

Additional concerns in DFAM include the dimensional tolerance capabilities of various 3D printers. The design is made to be printed on a Fortus 900mc. As per Stratasys specifications, this printer provides dimensional accuracy to +/- 0.089mm in the XY plane, as well as the Z axis, with additional tolerancing from slice height variation [11]. In general, our design tolerance requirements are somewhat loose since the device interfaces with soft tissue. The exception to this is the bony prominences which must be avoided by about 3mm. The design space has been generated prior to optimization to achieve this tolerance so the consideration needed not be factored into choice of print method.

The proprietary Windform series of polymers is printed inhouse at CRP Technologies on a Vanguard™ si2™ SLS printer. Generally, the process used by SLS affords greater control of properties, and therefore, accuracy of analysis given that the Z-plane mechanical properties tend to closely adhere to those of the print bed plane. Therefore, the consideration for full stress tensor characterization is not necessarily important.

2.8 CANFIT MODEL

The CAD models were first generated on CANFIT for its abilities to quickly generate complex organic surfaces. They were then input into Hyperworks for geometry optimization. The process of creating the CAD models is defined in the steps shown below.

CANFIT is the program that is used to create the basic geometry for the AFO models, after which the models are inputted into Hyperworks to be optimized. Firstly, the patient's foot and leg contour geometry must be inputted into CANFIT to create the inside surface of the AFO model. This process is done using a cast of the patient's foot/leg, which is then scanned using the 3D handheld Spectra^{TM} scanner shown in the 2.8.2. The scanned model is then offset at the vulnerable locations such as the ankle and first and fifth metatarsal, to avoid any rubbing or discomfort in those critical areas as shown in *Figure 21*. Finally the trim line is added to shave away unwanted material after which, the model thickness can be defined as shown in *Figure 23-Figure 30*. These final CANFIT models are then transferred to Hyperworks, in which they will be optimized for thickness and strut widths.

A detailed section for each of the steps taken, from creating the cast to having a model ready for Hyperworks will be discussed below.

2.8.1 CREATING THE CAST

The table below defines the consecutive steps that are taken to create a scan-able cast of the patient's leg/foot.

TABLE XI: STEPS TO CREATING THE FOOT/LEG CAST.

Step	Process	Description
1.	Put sock over the patient's foot.	This sock will prevent the cast from sticking to the patient's leg/ foot, as Shown in *Figure 16-Figure 18*.
	Mark all the vulnrable areas on foot/ leg.	Fibular head, ankle, Fifth and first metatarsal, as shown in*Figure 16-Figure 18*.
2.	Hold the tube over the sock.	This will give a guide line for cutting the cast off of the leg.
3.	Put cast on and wait for it to harden.	Give the cast a few minuits to fully cure, as shown in *Figure 19*.
4.	Cut the cast along the tube.	Use the tube as a guide and cut the cast off of the leg.
5.	staple the it back together.	This will enclose the cast back into a tubular r.
6.	Cast process is complete.	Cast is ready for scanning.

Shown below are the images taken from the cast creating process.

Figure 16: Cast sock marking fibular head and ankle.

Figure 17: cast sock marking first metatarsal and ankle.

Figure 18: cast sock marking fifth metatarsal and ankle.

Figure 19: Cast ready for cutting.

In general, the cast creating process was fairly quick, it took roughly 20 minutes from start to finish.

2.8.2 INPUTTING THE CAST GEOMETRY INTO CANFIT

After creating the cast, it can then be scanned with the 3D handheld Spectra™ scanner shown in Figure 20, and then uploaded as a CAD model in CANFIT. The scanning process is straight forward, simply aim the scanner at the cast, then press and hold the scanning button. The CANFIT model will be generated after the inter cast has been scanned.

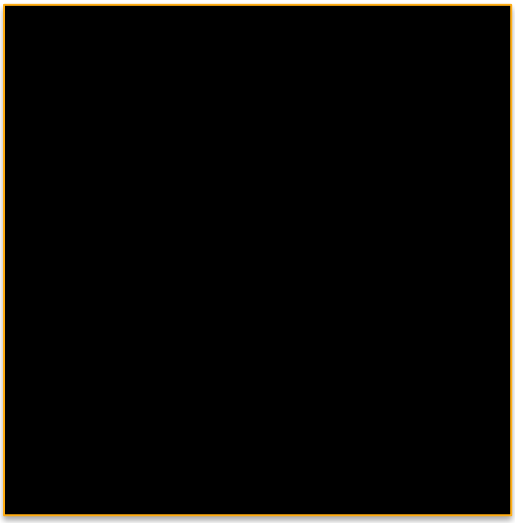

Figure 20: 3D handheld Spectra™ scanner.

2.8.3 CREATING THE CANFIT MODELS

Scanning the cast and offsetting the model will generate a base AFO design, that fits the patient foot/ leg contours. This base design will then be trimmed and flared to create four different designs. A base thickness is then added to create the design space for Hyperworks, as discribed in the table below.

TABLE XII: STEPS TO CREATING THE CANFIT MODEL.

Step	Process	Discription
1.	Offset the scanned model.	Create clearnces for the ankle, fifth and first metatarsal and the fibular head to avoid discomfort for the patient, as shown in *Figure 21*.
2.	Create net trimline.	The trimline will dictate the overall shape of the model, as shown inThe trimline will dictate the overall shape of the model, as shown in*Figure 22*
3.	Add flares.	The flares will round the edges of the AFO so they do not dig into the pateint's flesh and cause discomfort.
4.	Add thickness.	The thickness will initially have a uniform value of 6mm throughout the AF, which will then be readjusted to an optimal variable thickness by Hyperworks.
5.	End of process.	Models are ready to for Hyperworks, as shown in *Figure 23*-*Figure 30*.

Below are the figures of the four designs that were created using CANFIT.

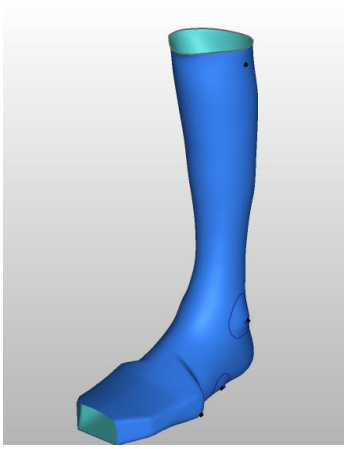

Figure 21: Offset cast model

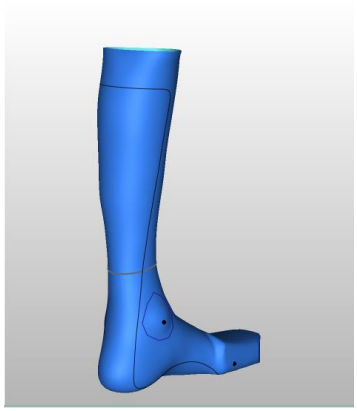

Figure 22: Defining the trim line

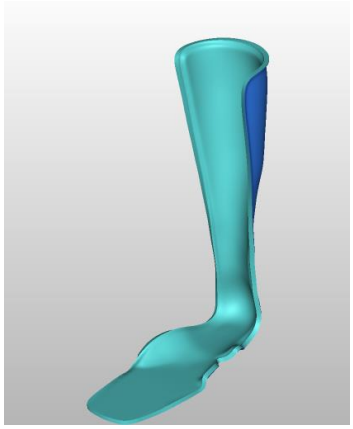

Figure 23: DES4 front view

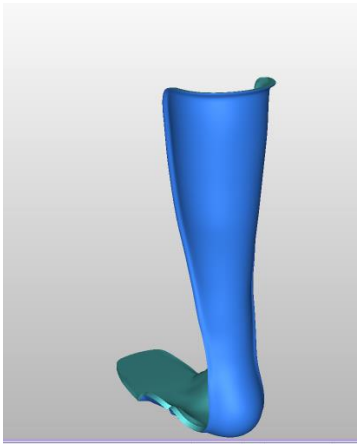

Figure 24: DES4 rear view

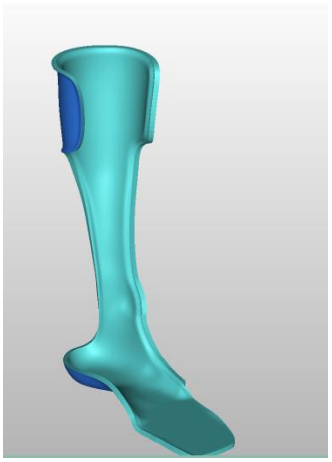

Figure 25: DES3 front view

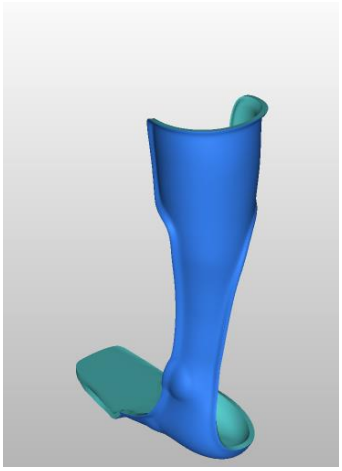

Figure 26: DES3 rear view

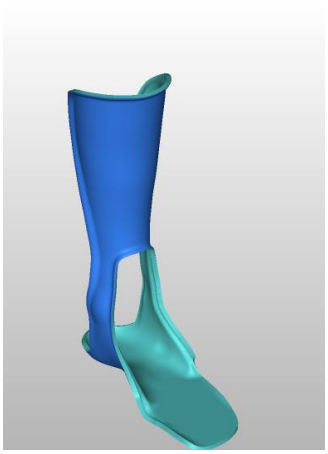

Figure 27: DES2 front

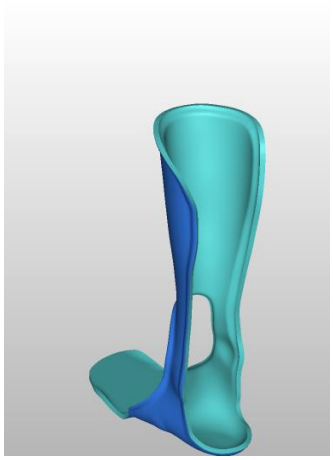

Figure 28: DES2 rear

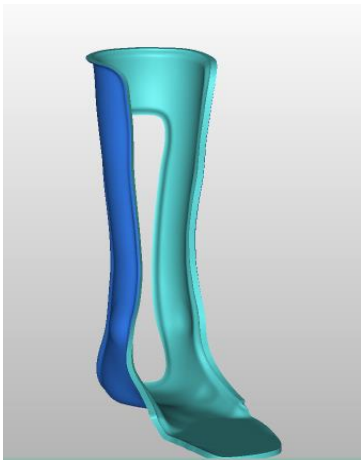

Figure 29: DES1 front

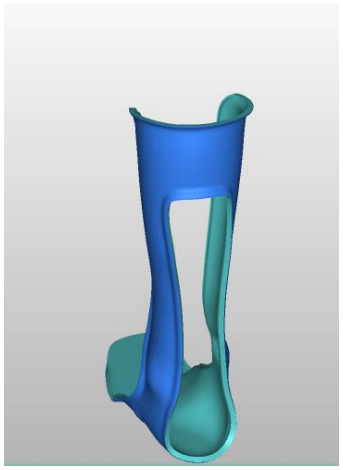

Figure 30: DES1 rear

3 DETAILS OF THE DESIGN

The final design features were derived from the list of customer needs discussed in Appendix A section 1.1. These needs where divided into five main categories which are; AFO is functional, AFO is durable, AFO is safe, AFO is easily manufactural, patient needs and AFO is comfortable.

The AFO design met the patient's needs by being discreet and aesthetically pleasing. Insuring that the AFO does not have any bulking geometry sticking out of the basic offset foot contour of the patient's foot did this.
We first started by importing a scanned cast model of the patient's foot, which was then used to define the foot contours of the AFO to insure that it will be comfortable. Moreover, the 3D model was then offered at vulnerable areas such as the ankle bone to insure that the AFO does not cause any irritation or discomfort for the patient. We also insured that the model was free of any sharp edges, which can cause harm to the patient.

For the AFO is functional category, we first defined that the AFO will help the patient simulate natural gate cycle. The AFO design does this by maximizing the forward propulsion, provide lateral stability, keep the patient's foot from dropping during the swing phase. The propulsion was maximized by incorporating the calculated stiffness target into the AFO design. The stiffness target was reached by optimizing the AFO's locations of deflection, the wall thicknesses and the locations and size cut outs where stresses are low, using HyperWorks. The design also had to accommodate for the fastening method which consisted of a Velcro strap that will be attached to the top section of the AFO as shown. The AFO also had to be easily applied and removed, which was easily achieved since the AFO design was not very confining.
Taking all the failure modes into account and also considering all of the load cases insure the AFO safety and durability. The different failure modes include maximum stress, fatigue stress criteria that were set through the material properties, then then AFO was optimized so the maximum stress values did not pass the stresses that where defined by the fail criteria. Also a safety of factor was incorporated into the design to insure the safety of the patient and the durability of the AFO.
The AFO also needed to be easily manufacturable, which was insured by using a 3D printer to produce the final product. Using 3D printing means there will not be any labor or detailed manufacturing instructions that makes the manufacturing process much simpler. The only constraint with 3D printing process was the printer print volume, which was not very limiting for our design because the company (Windform) we chose to get the 3D printing done at had a fairly large print volume which was able to fit the AFO design.

3.1 TOPOLOGY OPTIMIZATION

The FEM approach sought for this design involved the use of topology optimization. This approach is the preferred method to design for 3D printed components due to its ability to provide a designer the tools to optimize for performance or weight, given the freedom that the AM approach affords in manufacturing. Topology optimization requires confidence in FEM load cases, but provides versatility in generating atypical, organic surfaces, and is powerful in that the optimized part can be designed for geometric stiffness. For the design of a rigid AFO, this is the most appealing approach outside of iterative prototyping, which is significantly more expensive and would require more rigorous patient involvement.

Additionally, this problem involves the combined effects of anisotropic polymeric filament behavior and nonlinear geometric deformations in a dynamic context. The complexity of the design scenario meant that it was desirable to match that complexity in analytical rigor. However due to significant time constraints, some of these complicated factors were not included in our analysis, and were instead accounted for through approximations and assumptions. Some key assumptions made in the Hyperworks model are as follows:

- Isotropic material
- Linear elastic behaviour
- Load application through rigid connections
- Perfectly rigid boundary conditions

To achieve relative confidence in simulation results, a software environment combining optimization and FEA solvers was chosen, specifically the Optistruct solver, which is built into Altair's Hyperworks package. The software offers advantages in its ability to run iterative load steps, and create iso-clipped surfaces which dictate where elemental density can be reduced in a structure based on optimized load paths.
Hyperworks is unitless, so the units of measure are defined by the base unit that the model was created in. All models were designed and exported to Hyperworks in units of millimeters, so the equivalent unit system for the models within Hyperworks are shown in Table XIII

Table XIII: Equivalent unit system for Hyperworks models.

	Parameter	Units
Base Units	Length	mm
	Mass	kg
	Time	s
Derived Units	Force	mN
	Density	kg/mm^3
	Stress	kPa

The topology optimization process was conducted for two out of the four design concepts modelled in CANFIT. Ideally, the design process would involve optimizing all of the design concepts in order to determine which design's performance would most closely match our targets. However, due to a limited timeline, only DES3 (Asymmetric Lateral Strut Design) and DES4 (Posterior Strut Design) were analyzed in Hyperworks. The justification for further analyzing these two designs over the others was because of their simplicity in geometry. As it was already established that time was a large constraint on this project, it was decided that the simpler geometry would subsequently result time savings during the modelling, meshing, and finishing processes. Additionally, the simpler geometry would cut down on computation time, resulting in more time to be allocated towards achieving a detailed and thorough analysis. Figure 31shows the two concepts, DES4 and DES3 in the Hyperworks environment.

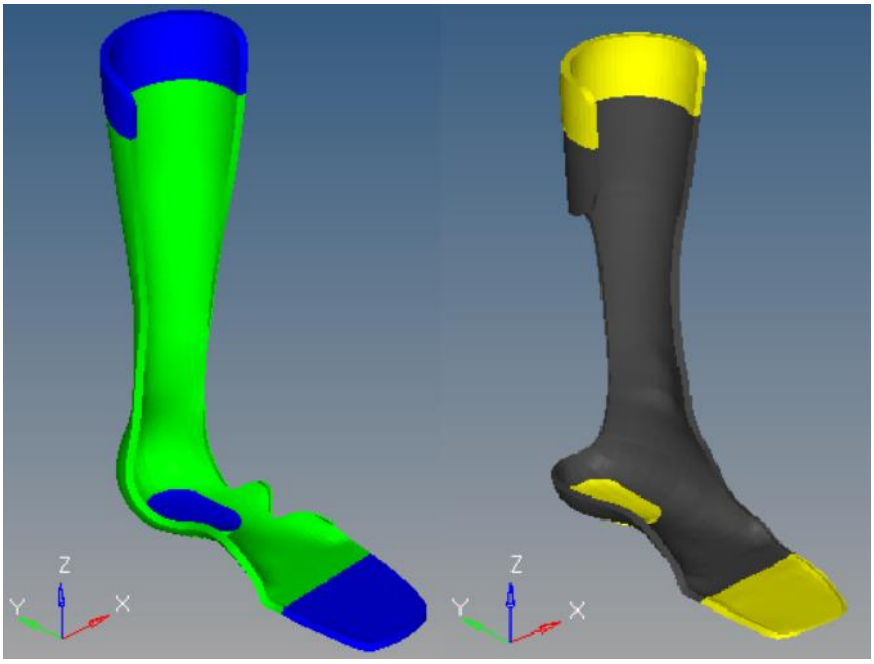

Figure 31: DES4 (left) and DES3 (right) in the Hypermesh environment.

The coordinate system used in Hypermesh shows the z-direction pointing vertically upward along the strut, the y-direction is directed along the length of the footplate pointing towards the heel, and the x-direction is pointing laterally outward. This coordinate system will be referenced for the duration of this section.
There are many parameters and factors that influence the likelihood of success in a topology optimizations study. Some key influencing factors discussed in this section of the report are:

- Initial geometry
- Selection of design and non-design space.
- Mesh type and mesh quality
- Material type and material properties
- Analysis type
- Load magnitudes and vectors, and the method of load application
- Boundary conditions and restrictions on degrees of freedom
- Optimization objective
- Design constraints and allowable deviations
- Optimization convergence criteria
- Optimization Control Cards

Due to the fact that there are so many parameters which impact the success of the optimization study, many permutations of the study were performed before feasible and sensible results were obtained. The subsequent sections highlight the results and parameters from the specific study that yielded the most successful and realistic results. Ideally, the topology optimization process would yield a singular result that could then be modified and cleaned up such that it is comfortable and safe for the patient to wear, while still maintaining strength and performance characteristics. Initially this was the intent of the topology optimization process. However, due to a multitude of unforeseen setbacks and roadblocks, the topology optimization was simply used to determine the topology which optimizes the resulting load paths that result from the applied external forces on the AFO. The optimized load paths were then used as a starting point for re-constructing a final model that could be printed within the imposed budget constraints for the project.

3.2 DESIGN SPACE AND NON-DESIGN SPACE

One of the most important and influential factors for running a successful topology optimization study is selecting the appropriate design space (DS) and non-design space (NDS), and requires consideration for the functionality of the finished design. The non-design space was classified as any region of the design that we did not want to include in the topology optimizations study. Since the topology optimization process will only remove material from the design space, it follows that any region identified as non-design space would retain its original geometry in the final design.

Figure 32 shows the design space in green and the non-design space in blue for the DES4 concept model. There were three regions specified as non-design space in each topology optimization study: (1) the fixation point at the top of the strut where the AFO will be mounted to the patient's calf via a Velcro strap, (2) the heel region of the footplate, and (3) the toe region of the footplate. The design space for both devices consisted of all remaining regions including the majority of the strut as well as some sections of the footplate. The selection of design space and non-design space is highly influential on the topology optimization results achieved, and it was therefore very important to make appropriate selections. Increasing the amount of non-design space present in the model can impose unnecessary constraints on the topology optimization study, and can contribute to an infeasible solution. It is for this reason that we attempted to select small regions of non-design space in order to ensure that the optimization study was not unnecessarily limited.

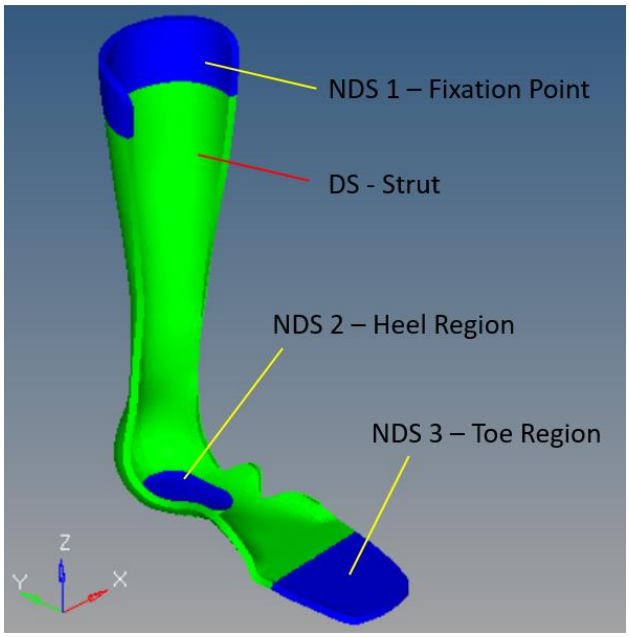

Figure 32: Design Space (green) and Non-Design Space (blue) for DES4 in Hyerworks.

3.3 MESH GENERATION

In FEA theory, a shape function is regarded as the expression that describes the ability of an element to provide a space-specific solution for a load type, and is dictated by the type of element being chosen. For proper analysis, the differential of strain across the element should be an accurate representation of the physical strain distribution of the material at that location. Given the application of an AFO, deformation distribution in a bending-dominant load case is calculable according to the matrix:

$$EIy = -Fx^3/6 + F^2x/2 - FL^3/3$$

Where y is the deformation in the transverse direction, and F is the cantilever load applied.

If we differentiate this expression for change in y along x, we get a 2nd order polynomial. Therefore, a discretized strain distribution solution for bending stress should utilize elements with shape functions (N) that when fit end to end can approximate the parabolic curve of strain distribution in a cantilever load case.

Given the fact that stress depends on strain and an, its result as a representation of material failure is dependent on the precision of the mesh. With this knowledge, and the

limitation of student-available FEA methods like Hyperworks Student Edition, results depicting deformations will tend to be more reliable, whereas stress values are those affected most by mesh quality issues. To curb the effect of inaccurate discretization of stress distribution, the elements were chosen as 8-node CHEXA elements that provide the following shape function [12]:

$$Shape\ N_n^e\ =\ (1/8)(1\ -\ z)(1-\eta)(1-\mu)$$

Where along with the nu and mu symbols represent the natural coordinate system for the element, ie, that which shifts along with deformation of the element itself, and is scaled to range from [-1,1] for each case. The import takeaway is that the shape functions, which describe the deformation in Hexa8 elements, do not contain second order terms with respect to any axis.

Notably, these elements are 1st order, and do not match the 2nd order strain distribution of the strain exhibited. However, with adequate precision, the hexa elements are able to capture the information within reason. It is desirably to choose low order elements when computation constraints are an issue, as is the case here, but it is assumed that discrepancies are accommodated in the safety factoring of the device.

If we differentiate the expression for N above, the result of this gives an expression for the change in shape exhibited by an element, known as the *Jacobian.* For this analysis, repeated checks of context-specific Jacobian magnitudes was conducted such that it could be ensured that the mesh was not excessively warped and therefore could be said to be yielding reasonable strain results. For this reason, a solid mesh using TETRA4 and HEX8 solid elements was utilized.

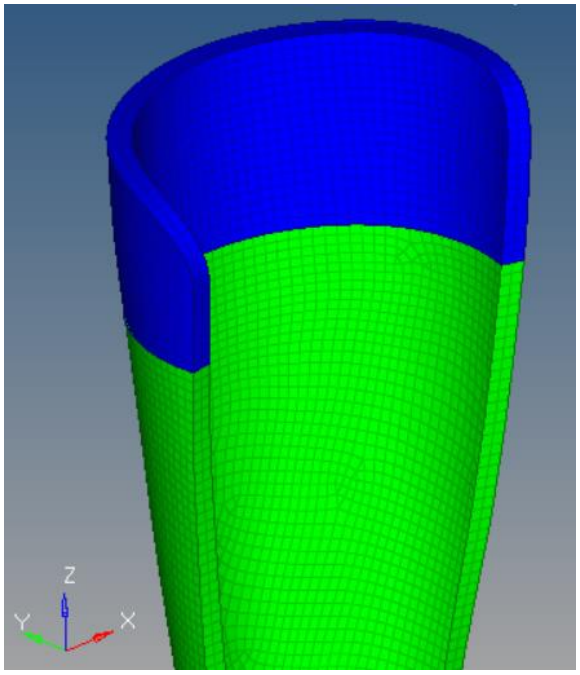

Figure 33: Detail view of final mesh for the upper half of DES4 in Hyperworks.

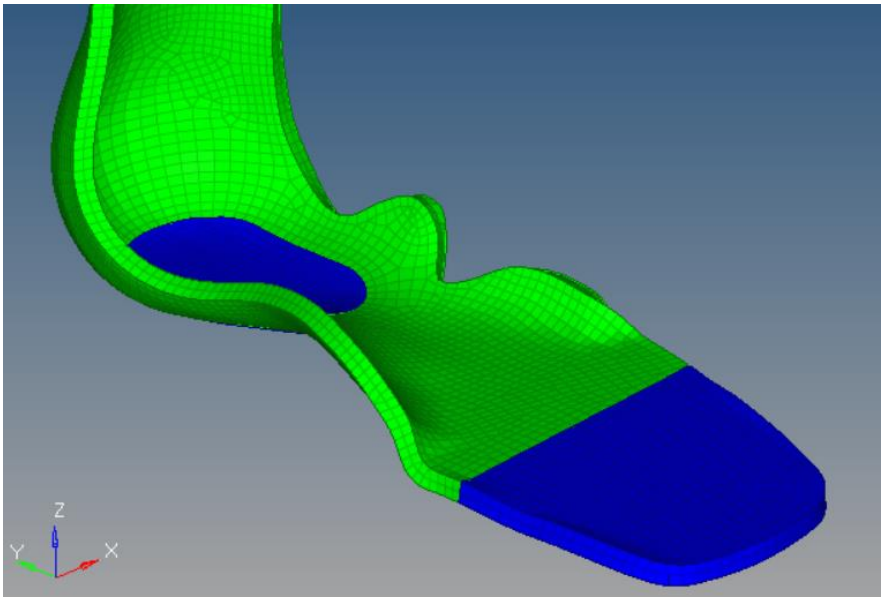

Figure 34: Detail view of final mesh for the lower half of DES4 in Hyperworks.

3.4 Effective Material Properties

After the solid mesh was created, the next step in setting up the optimization study was to enter the effective material properties. Effective material properties are relevant for materials that are anisotropic in nature, and have been reoriented in 3D space. Two

applications that the concept of effective properties is commonly used in are composite laminates and 3D printed parts.

In absence of print volume constraints for all materials considered, and for the purpose of comparison, it was assumed that the optimal print orientation could be achieved for all materials, and therefore material properties were taken to be their maximum posted values. In reality, print volume could potentially limit the possible print orientations. If this is the case, a compromise must be made between orientations that would improve the strut stiffness, versus an orientation that will fit within the specified print volume.

3.5 Boundary Conditions and Load Application

Load application and boundary conditioning was done with various techniques to assess their validity. In Hyperworks, loads can be applied as distributed pressures to varying element distributions, as well as distributed loads applied to a single central node that redirects the load to the desired surface. For boundary conditioning, consideration had to be made for how the device would be used. For example, experimental GRF data for the patient indicated a floating CoP that transitioned from the heel past the arch of the foot to the pad of skin just before the toes.

For the purpose of improving computation effort and FEA convergence probability, and to simplify the analysis, the team assumed that the inertial effects can be treated as quasi-static and the dynamic load cases were deconstructed into a series of discrete static loads. The kinematic model covered in Section XX, allowed us to do just this. The inertial effects are captured within these calculations, so we considered this approach acceptable.

3.5.1 Dynamic to Quasi-Static Load Approximation

The process of approximating a dynamic loading scenario as a static problem involves dividing up the dynamic case into a series of discrete quasi-static load steps, where the D'lambert Force represents the instantaneous inertial force as the time derivative of an object's momentum, expressed for a particular instance in time.

The time-dependent load cases identified using the patient's kinematic model were identified in 2.2.2, and from the results of the kinematic and dynamic patient model several load cases of interest were singled out. The discrete load cases in Table XIV were determined based on the critical stages of gait, and were selected to encompass all loading conditions for regular device use. Load Steps 1 through 5 were applied

sequentially in order to illustrate the device's deflection performance trends over time as the patient applies loads through their natural gait cycle.

Load Steps 5 and 6 are shown in parentheses, as they are used to determine the device's performance and structural integrity under irregular loading. Load Step 5 is the potential strut torsional load due to side loading on the footplate, and Load Step 6 is an estimate of the torsional load experienced by the footplate when the device is in use over rough terrain. Notably, the peak load considered occurs a contralateral heel strike, at which point load is transferred from one foot to the other.

Table XIV: Loading scenarios used for FEA and topology optimization.

#	Load Step	Applied Force	Boundary Condition	Used on study
1	Heel Strike (initial contact)	37 N	Fixed support at heel region only	FEA Re-analysis
2	Loading Response (flat foot)	45 N	Fixed support at heel and toe region	FEA Re-analysis
3	Mid-stance	53 N	Fixed support at heel and toe region	FEA Re-analysis
4	Contralateral Heel Strike	83 N	Fixed support at toe region only	Topology Optimization
(5)	Footplate Torsion Load	65 N	Fixed support at toe region only	FEA Re-analysis

Keeping with the two-dimensional approximation of gait motion, all load steps were applied along vectors which lie on the mid-plane of the foot, with the exception of the torsion load, which is applied perpendicular to the mid-plane of the foot. Diagrams for each load step are shown in Figure 35 through Figure 39.

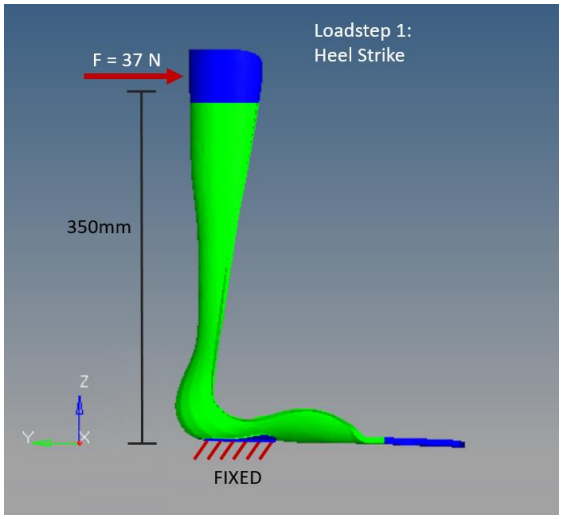

Figure 35: Diagram of heel strike load scenario.

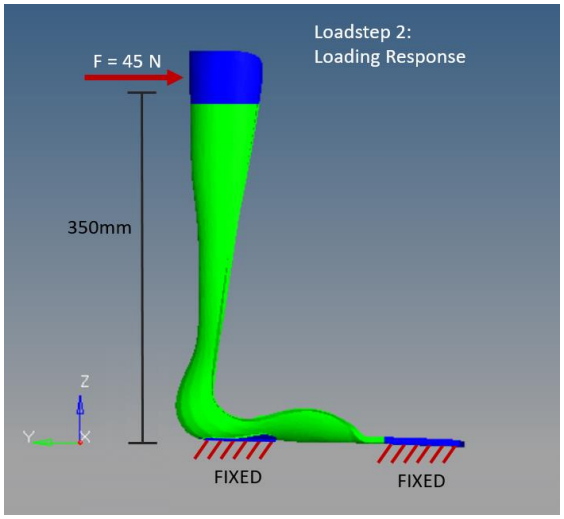

Figure 36: Diagram of loading response load scenario.

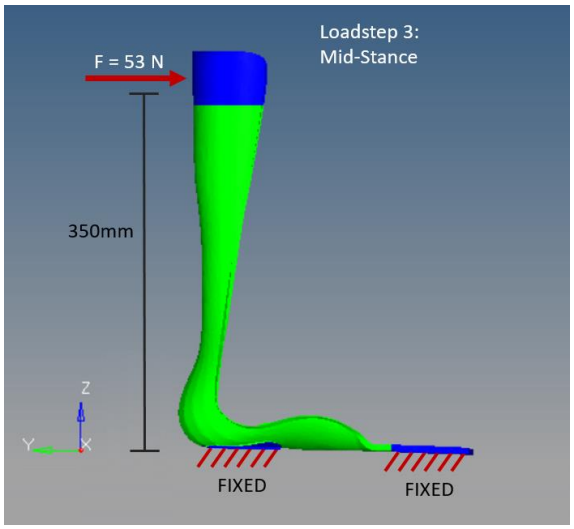

Figure 37: Diagram of mid-stance load scenario.

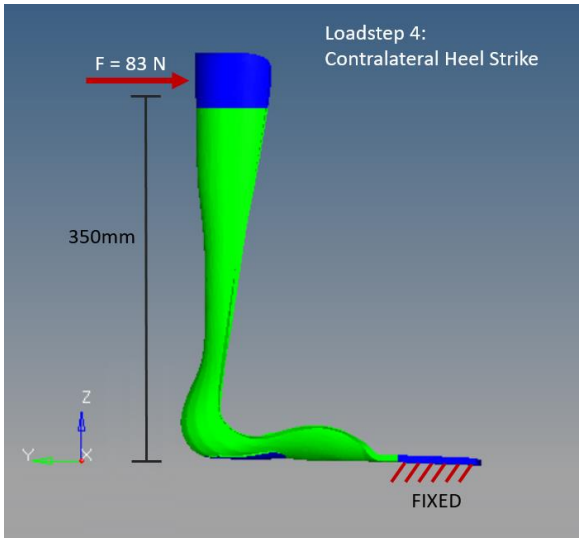

Figure 38: Diagram of contralateral heel strike load scenario.

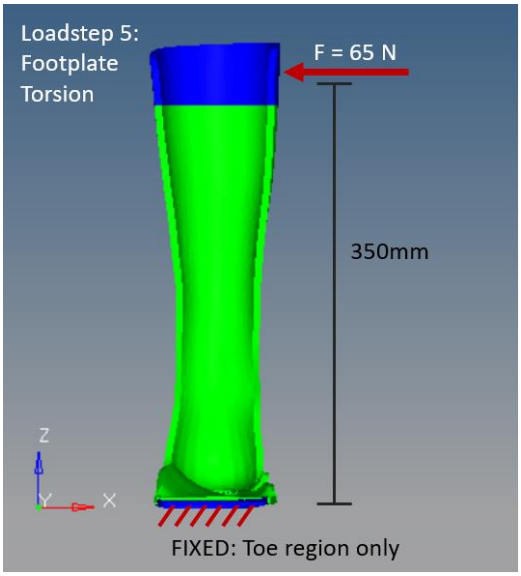

Figure 39: Diagram of footplate torsion load case.

It is important to note that during topology optimization, only Load Step 4 (at contralateral heel strike) from Table XIV was used to generate the optimized load paths for topology optimization, since this is the load case that was deemed to be most important to consider in terms of performance. All other load steps were used as checks in the FEA reanalysis stage after the preliminary topology results were obtained. This was done to save time during computations and to reduce the risk of non-convergent optimization results. In the future, it is recommended that all load cases be considered during the topology optimization process in order to create a more all-encompassing solution.

3.6 Optimization Parameters and Constraints

There were many different approaches devised to solve the problem of topology optimization. Table XV highlights the optimization parameters used for the first attempt at running the topology optimization study.

Table XV: Initial topology optimization parameters entered into Hyperworks.

Parameter	Description
Material selected	Various.
Load Applied	Loading during contralateral heel strike, -83 N applied in the y-direction (perpendicular to the AFO strut), located approx. 14" from the base of the heel.
Boundary Condition	Fixed geometry at the toe region of the footplate (all DOF constrained).
Stress Constraint	Maximum stress > 0.397 x yield stress of the material.
Deflection Constraint	Deflection target of 160mm at the point of application of the load (to achieve an effective linear stiffness of 1.31 N-m/deg).
Optimizing Objective	Minimize total mass.
Topology Optimization Code	Optistruct.
Study Type	Linear-static.

The study was conducted for a wide variety of 3D printing material options due to uncertainty in the feasibility of each material. The materials considered were: PC-ISO, Ultem 9085, Ultem 1010, 3DXTech CF-PETG, and Windform SP. Material properties for these and other materials considered can be found in Table 9. The optimizing load condition was that of contralateral heel strike, for which the performance stiffness target was based on. Since contralateral heel strike normally occurs after the heel has raised off of the ground, the boundary condition was applied to the toe region only. This assertion was confirmed through the gait kinematics and dynamics analysis conducted, which showed that the point of application of the GRF was ahead of the MTP joint during contralateral heel strike. The stress constraint was material dependent, and a safety factor of 2.52 was used based on Section 2.6. The deflection constraint was derived from the gait kinematics and dynamics analysis, which stated that the optimal torsional stiffness of the AFO must be approximately 1.31 N-m/deg.

The optimizing objective was to minimize total mass. Minimizing total volume is also a valid optimizing objective, and would yield the same results since the AFO is assumed to be of solid fill and uniform density. Another common optimization variable is compliance, which refers to the distribution of strain energy density throughout the part, however unsuccessful in producing a feasible result using this method.

Specific to Optistruct and RADIOSS, the two solver tools in Hyperworks, there are many possible optimization methods, with different strengths and limitations in each case. Three relevant optimization cases are linear static analysis, non-linear geometric analysis, and dynamic analysis. Linear static is not ideal for predicting accurate deflections of high strain designs. Imposing a required stress or deflection target on the mesh can create distortion of the elements as they attempt to achieve the required targets within the limited relative nodal constraints. In doing so, the extreme Jacobians produced can be mathematically inaccurate. As mentioned previously, the dynamics of human gait motion was approximated using a quasi-static assumptions, where discretized load cases were determined, and will be applied in place of a fully dynamic study.

It is the case that the deformations desired of an AFO design containing a rigid strut and flexible MTP region at the imposed timing of max deflection (during contralateral heel strike) tend to push the resulting deflections outside of the assumed linear small-angle deformation range assumption required for the linear stress-strain relationship according to Hooke's Law to remain valid. With this in mind, the strongest approach is simulated application of Finite Strain Theory (FST) through a non-linear geometric analysis, which is a more general case for elements deforming with variable stiffness. It was therefore decided that a geometric non-linear study is the most accurate method for simulating AFO deflections. However, due to limited time constraints, computation power, and access to appropriate troubleshooting resources for Hyperworks, the non-linear analysis, though attempted, was not fully implemented. Therefore, the problem was approximated using a linear-static approach.

3.7 Adapted Optimization Approach

From the preliminary results of the optimization study there were many lessons learned. It was found that, for the given design space, certain constraints were impossible to satisfy for a number of reasons. It is often the case with optimization problems that, given a set of parameters, variables, and constraints, often the result is an infeasible design, with no optimal solution. This was the case for the initial set of optimization attempts. Given the design space as a starting point, the materials available, the stiffness targeting for optimal gait, and the desired safety factor, a feasible solution was not initially achieved for both DES3 and DES4 concepts, with any of the materials

chosen. One root cause for the initial failed optimization attempts was that the constraints were too limiting.

In the face of failing optimization attempts, and a fast-approaching design deadline, the optimization approach was adapted. For the purpose of achieving a convergent optimization solution, the deflection constraint was removed, and allowable margins for stress were widened. This was done with the intention of obtaining results that could then be interpreted and applied to future design modifications. It is important to note that the results obtained and discussed in this section are not those of a fully optimized and manufacturing-ready design, but rather the results of the first step towards achieving a feasible design in a larger optimization problem. The results shown highlighted in this section, along with the recommendations discussed in 4.1, are intended to lay the foundation for future optimization steps, such that this project can be continued in the future and the approach can be perfected.

3.8 Preliminary Topology Optimization Results

The first successful result from the optimization process was achieved using the material Windform SP. Isometric, front and side views of the topology optimized model (using an iso-clipped value of 0.0725 or 7.25%) for the DES4 concept are shown in Figure 40 and Figure 41.

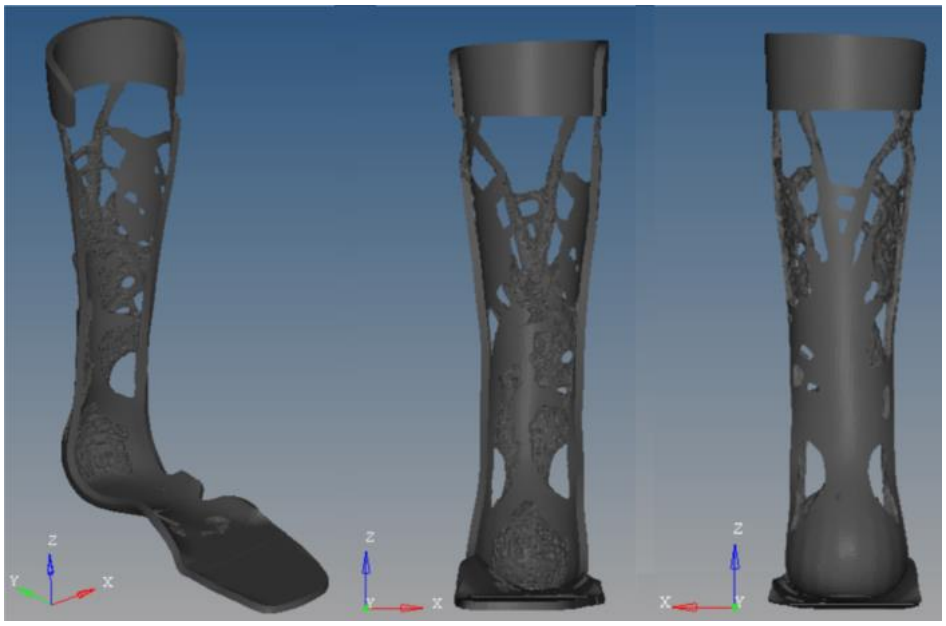

Figure 40: Isometric view (left), front view (middle), and back view (right) of topology optimized Windform SP AFO in Hyperworks, with 7.25% iso-clipping.

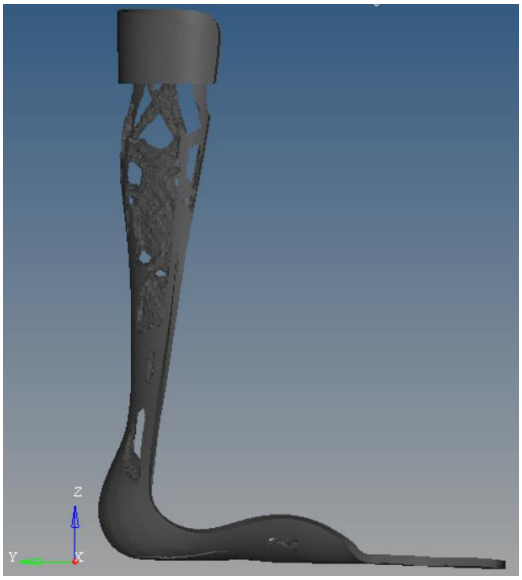

Figure 41: Side view of topology optimized Windform SP AFO in Hyperworks with 7.25% iso-clipping.

The topology optimization process yields not just one design, but one element density plot, which can be modified using the iso-clipping function in Hyperview. The element density plot for the topology optimized version of DES4 using Windform SP is shown in Figure 42. The element density plot is unit-less, and provides a means of determining the critical locations on the part for which material is needed to sustain the loads applied

and to achieve the desired performance. An element density of 1.0 (red regions) indicates that material is required, and an element density of near-zero (blue) indicates excess material that can be removed. Effectively, the results produced from the topology optimization process indicate the optimized load paths for stress to be distributed throughout the part. The iso-clipping feature allows the user to gradually remove material in regions where it is not required (the blue regions in Figure 42), in order to achieve a design that is both realistic and functional. For this particular case, an iso-clipping value of 0.0725 was used to achieve reasonable results.

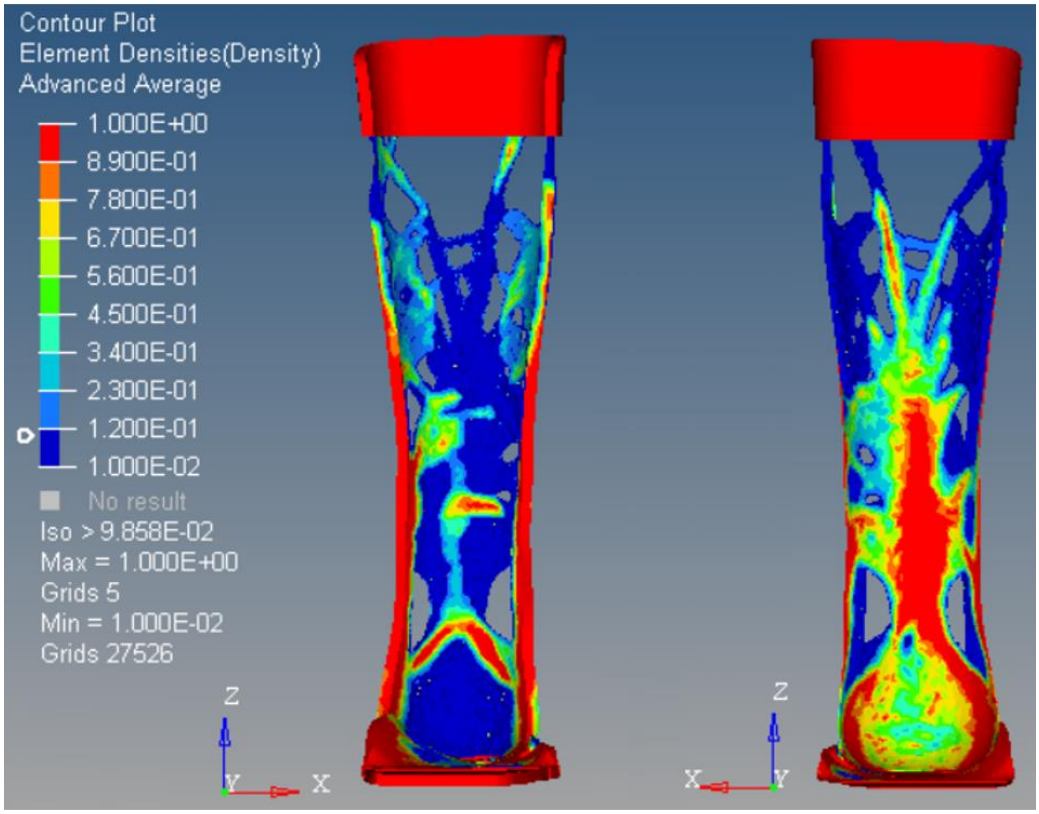

Figure 42: Element density plots for the front (left) and back (right) views of topology optimized Windform SP AFO in Hyperworks, with 7.25% iso-clipping.

After achieving a reasonable topology result using the iso-clipping feature in Hyperview, the next step in the process involved re-meshing the new optimized geometry, and re-running the FEA using identical loading conditions to investigate how the new iso-clipped design will perform under the same load in terms of stress and deflection. Hyperworks has a built-in function that allows the user to achieve this, called OSSMOOTH. This function smooths out the tessellated surfaces generated from the topology optimization process, and generates new “clean” geometry and re-meshes the new geometry based

on the previous mesh. In this context, “clean” geometry refers to that which does not have any significant sharp corners or floating elements left over from the iso-clipping process. The un-deformed stress contour plots resulting from the FEA re-analysis process are shown in Figure 43, Figure 44, and Figure 45. The stresses shown in the contour plots are in units of kPa, and the plots are scaled to show the peak value as the maximum stress in the part.

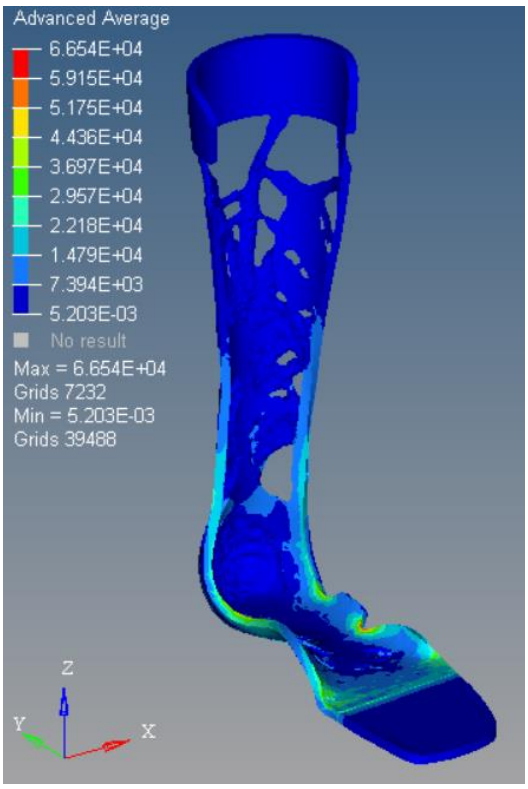

Figure 43: Overall stress contour plot for the preliminary topology optimized Windform SP design, in units of kPa.

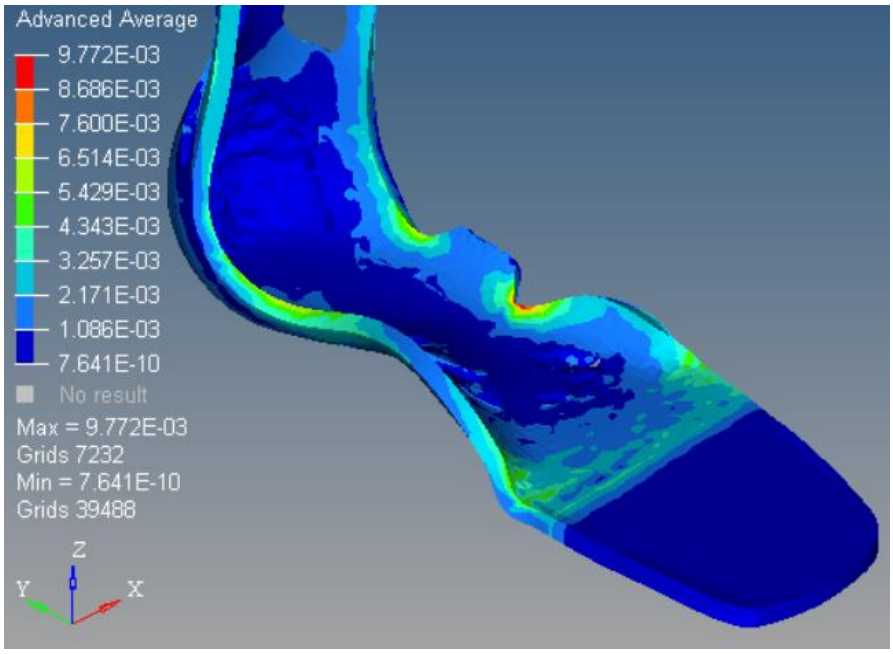

Figure 44: Footplate top detail view of stress contour plot for the preliminary topology optimized Windform SP design, in units of kPa.

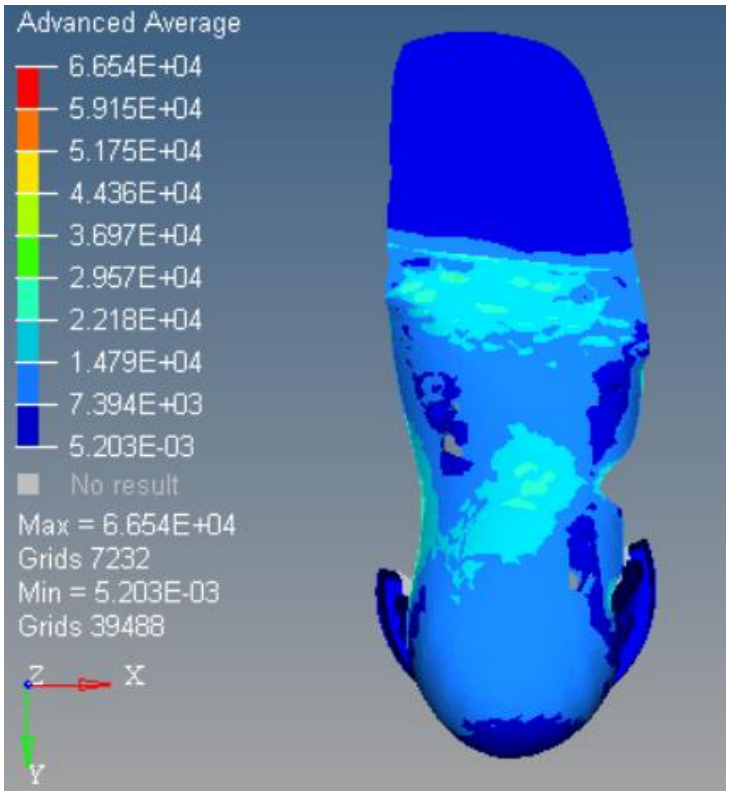

Figure 45: Footplate bottom detail view of stress contour plot for the preliminary topology optimized Windform SP design, in units of kPa.

Stress contour plots are shown in the averaged state, using the Advanced Average method, which averages the results at the stress tensor level, before VonMises stress is calculated. This is the recommended averaging method in terms of accuracy [14]. The contour plots reveal that the most highly stressed areas occur at the heel and MTP regions of the AFO, where geometry and cross-section changes occur. This is to be expected, as these geometric transition regions provide a means for stress to become concentrated.

Note that the tabulated yield strength of Windform SP is 76.1 MPa, and the maximum allowable stress was determined to be 30.2 MPa based on a safety factor of 2.52. There are still some locations on the AFO in its current state that have excessive stresses which exceed the allowable stress criteria used during optimization. This is due to the fact that the stress constraint was applied globally, and the optimization code does not look for localized stress concentrations to avoid intermediate errors in the solving process. As a result, not all stress concentration issues were addressed within the first iteration of topology optimization, and further modifications to the design are necessary in order to completely alleviate all high-stress areas. The process of smoothing and re-analysis is covered in 3.9.1.

Overall deflections were also plotted in the FEA re-analysis process to examine the AFO's combined material and geometric stiffness in bending under the prescribed load for the critical case of contralateral heel strike. Deflections contour plots, shown in Figure 46, are in units of mm, and the charts are scaled to show the peak value as the maximum overall deflection in absolute value. The preliminary design is represented in both un-deformed and deformed (1:1 scale) states.

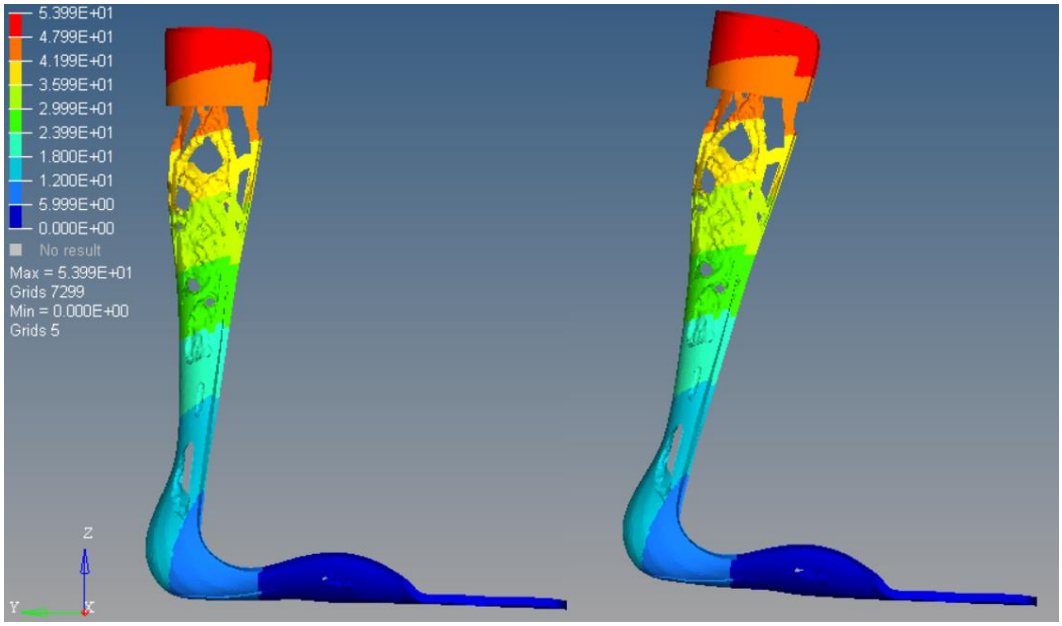

Figure 46: Side view of deflection contour plot represented in un-deformed (left) and deformed in 1:1 scale (right) states for the preliminary topology optimized Windform SP design, in units of mm.

The topology results were obtained for optimized the load paths, however due to this material's relatively high elastic modulus, the design was too stiff, and had to deviate from the deflection constraints imposed in order to pass the maximum allowable stress criteria. The optimized Windform SP design deflected approximately 54mm under the imposed load of 83 N.

3.8.1 Inadequacies with the Lateral Strut Design

The lateral strut design DES3 was the other concept selected for further optimization after the concept scoring process. Similar to the DES4 design, the topology optimization approach was also applied to the DES3 concept. Non-design space, load cases, and boundary conditions were kept constant so that a direct comparison could be made to the DES4 model. In all attempts at topology optimization, and with all of the materials chosen, none of the studies converged to yield feasible designs, even within the first iteration. This was a clear indication that the design space (or starting point) was not adequate to sustain the applied loads.

Further investigation revealed that excessive stresses and deflection were occurring in Iteration 1, before the optimization code even began removing material. The cause of the excessive deflections was suspected to be due to the nature of the asymmetric

design to tend towards lateral deflection when subjected to a bending load about the x-axis. In order to test this theory, a vertical load was applied in the center of the toe region of the DES3 AFO's non-design space based on GRF data collected from the patient. The load was applied upwards at 892 N and fixed at the cuff near the top of the strut. To keep the study directly comparable to the optimized DES4 model, Windform SP (one of the stiffer 3D printed materials considered for this project) was the material chosen for this investigative study. This new loading scenario is shown in Figure 47, where the applied load is indicated in green and the fixed constraints are indicated in blue, which apply to all internal nodes on the cuff non-design space. An FEM study was run to determine the x-direction reaction force at the top of the AFO strut, and it was found that the peak equivalent lateral load was 78000 mN or 78 N. This result is indicated in Figure 48, and illustrates a force contour plot in units of mN.

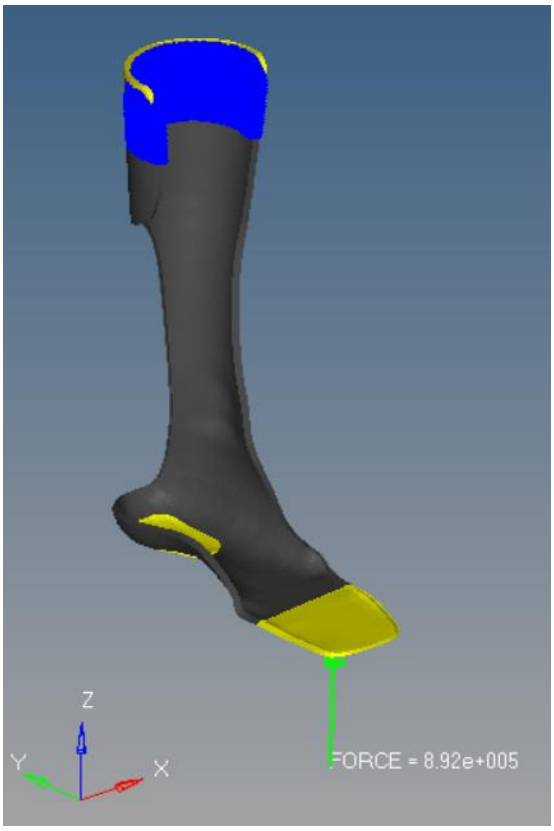

Figure 47: Investigative load scenario for DES3 showing applied ground reaction force in mN.

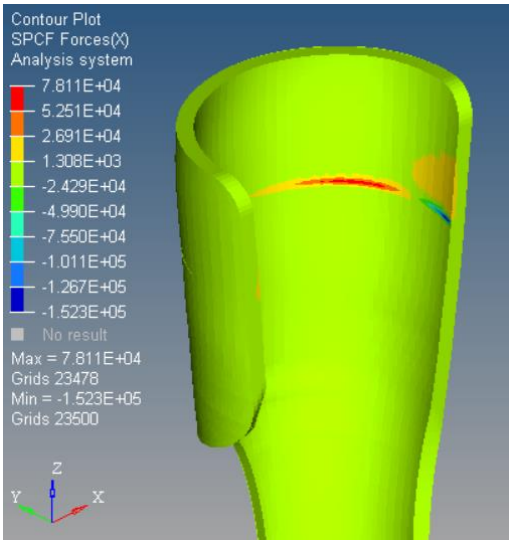

Figure 48: Peak reaction force in the x-direction at the AFO fixation point for an applied ground reaction force of 892 N on design concept DES3.

This reaction force of 78 N was then applied in the negative x-direction in a load case similar to the one depicted in Figure 39. The resulting deflections and stresses were plotted in Figure 49 and Figure 50 respectively.

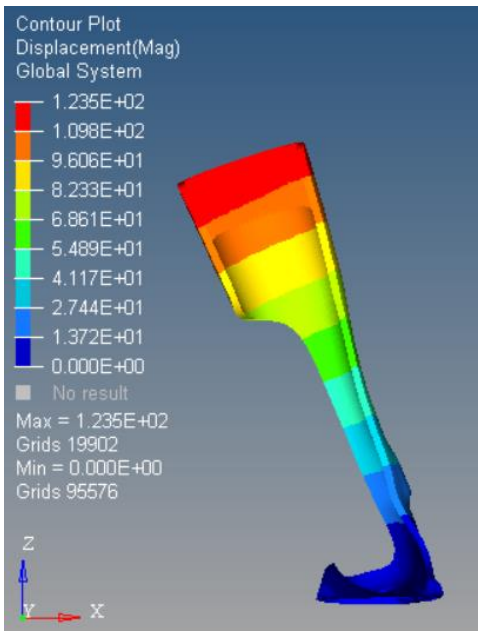

Figure 49: DES3 Windform SP model excessive deflections in mm (scaled 1:1 for visualization) due to equivalent lateral bending load of 78 N caused by GRF.

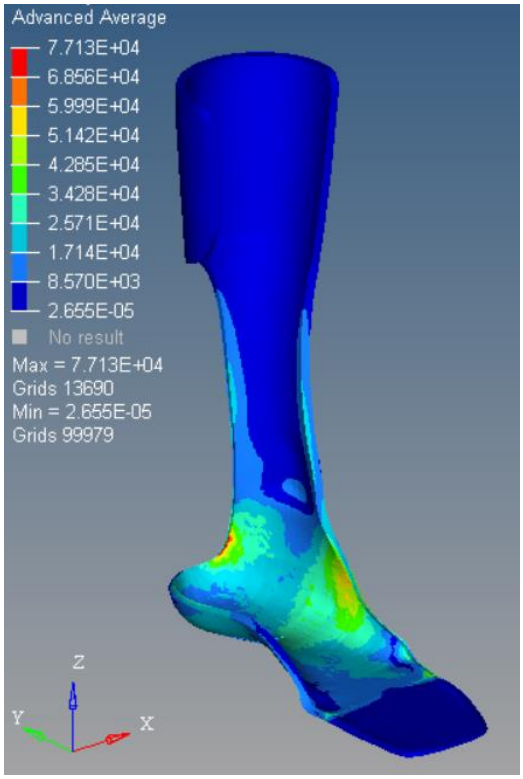

Figure 50: DES3 Windform SP model excessive deflections in kPa (un-deformed) due to equivalent lateral bending load of 78 N caused by GRF.

Based on the deflection contour plot in Figure 49, under the prescribed lateral load, the DES3 concept design experiences substantial deflections of up to 120 mm laterally, which was deemed to be excessive in terms of what would be allowable for facilitating healthy and comfortable gait.

Note that the deflection and stress contour plots are to be interpreted with caution, as it is likely that the problem has transitioned into the realm of non-linear geometry, however the general trend of large lateral deflections is apparent, and this was deemed sufficient evidence to rule out DES3 as a viable optimization starting point in its current state. However, this is not to say that a feasible result could not potentially be obtained if the design space for DES3 were modified to drastically increase lateral geometric stiffness. However, due to limiting timeline for this project, the design space and concept model for DES3 were not revisited.

3.9 Post-Optimization Refinement

Using Hyperworks, an optimized solution was obtained for the DES4 posterior strut using Windform SP material, however it was found that the optimized design still contained some regions of unacceptably high stress. Geometry smoothing was performed using Autodesk Meshmixer in order to smooth out the rough contours of the model and to eliminate stress concentrations in areas of interest. Most notably, contours in the footplate were slightly modified such that the changes in cross-section were more gradual, and certain load-bearing members were stiffened in an attempt to raise to safety factor closer to the desired value of 2.52.

3.9.1 FEA Re-analysis of Topology Optimized Design

Once the final geometry was generated using Meshmixer, the finite element model was created in Hyperworks using the shrink-wrap mesh function with an element size of 2mm to ensure that a fully enclosed solid mesh was achieved. Then, the FEA re-analysis was run for all of the load cases identified in Table XIV. This was done to ensure that the design was safe for the entirety of loading scenarios considered, and to identify the final deflection and stiffness characteristics of the AFO. While FEA was run for all five load scenarios, only the contour plots for the worse case-loads are displayed. Displacement contour plots (scaled 1:1) are shown in Figure 51, Figure 52, and Figure 53 for the Mid-Stance, Contralateral Heel Strike, and Footplate Torsion load steps respectively. It was found that under peak loading at mid-stance, the maximum deflection in the y-direction was approximately 8mm. Under peak overall loading during contralateral heel strike, the maximum deflection in the y-direction was 44 mm. This is substantially less than the ideal value of 160mm. However, engineering is about making trade-offs, and due to the limitations of the material strength and stiffness, a degradation in performance was acceptable given the importance of safety under the prescribed loading conditions. Under the lateral load case, deflections were limited to approximately 5mm, which was deemed to be acceptable in terms of facilitating natural gait, as these deflections would not significantly alter the gait characteristics of the patient during normal device use.

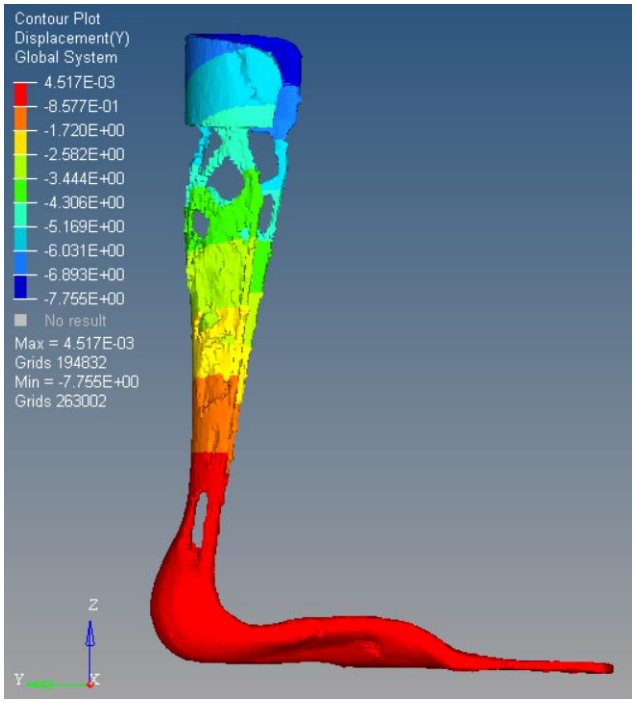

Figure 51: Refined AFO deflection contour plot (scaled 1:1) for the load case of Mid-Stance loading, with applied load of -53N in the y-direction.

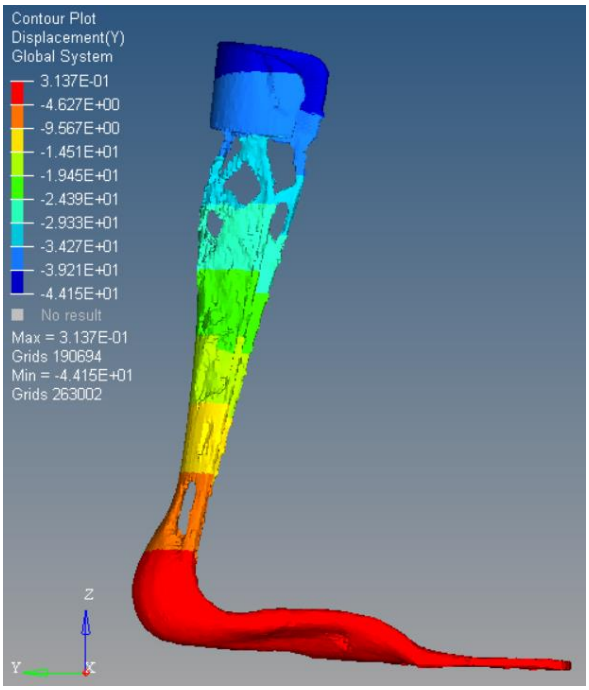

Figure 52: Refined AFO deflection contour plot (scaled 1:1) for the load case of contralateral heel strike loading, with applied load of -83N in the y-direction.

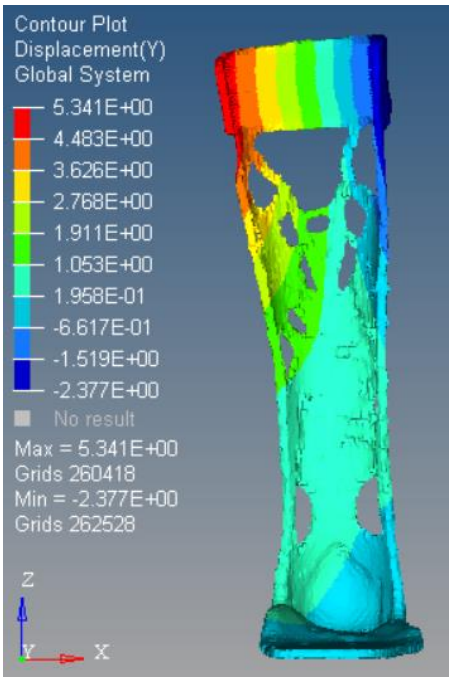

Figure 53: Refined AFO deflection contour plot (scaled 1:1) for the load case of lateral loading, with applied force of -65N in the x-direction.

In addition, the final stress contour plots were generated for all five load cases, however only the FEA results from the worst case load scenario are presented. These plots of VonMises stress are shown in Figure 54, Figure 55, and Figure 56 for the load cases of mid-stance, contralateral heel strike, and footplate torsion respectively. It was found that the peak stress for all load cases was 56.4 MPa, which occurred at the foot-plate near the point of application of the fixed boundary condition near at the toe region. This peak stress value resulted in a factor of safety of 1.31, which is notably lower than the safety factor prescribed in 2.6. Note that stresses observed in the vicinity of an idealized boundary condition can often be misleading, and it is possible that the exceptionally high loads experienced in the footplate region are a product of the idealized rigid boundary condition applied in the contralateral heel strike load step. It is for this reason that the excessive stresses in this region are deemed acceptable despite the low safety factor. However, this discrepancy between ideal and actual safety factor indicates that there exists an opportunity for further refinement of the design in order to achieve more optimal performance under the given loads.

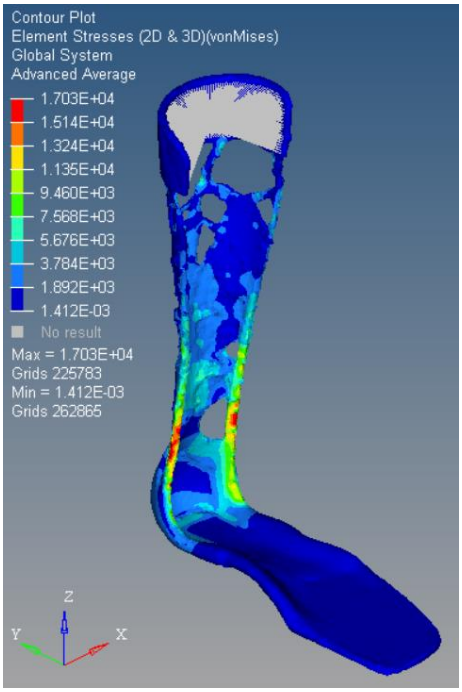

Figure 54: VonMises stress contour plot for FEA re-analysis in MPa on mid-stance load case.

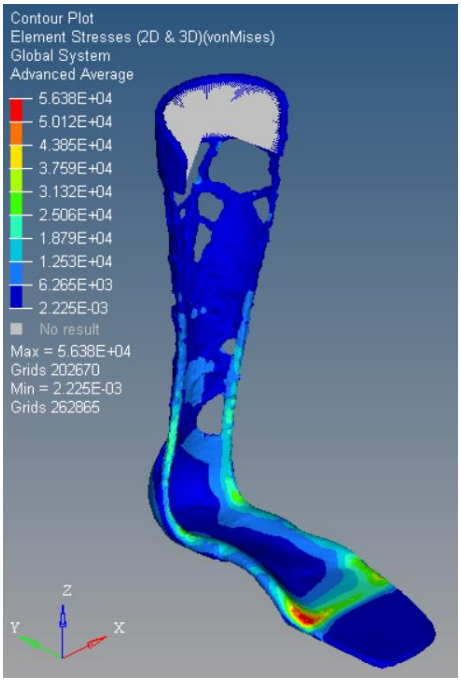

Figure 55: VonMises stress contour plot for FEA re-analysis in MPa on contralateral heel strike load case.

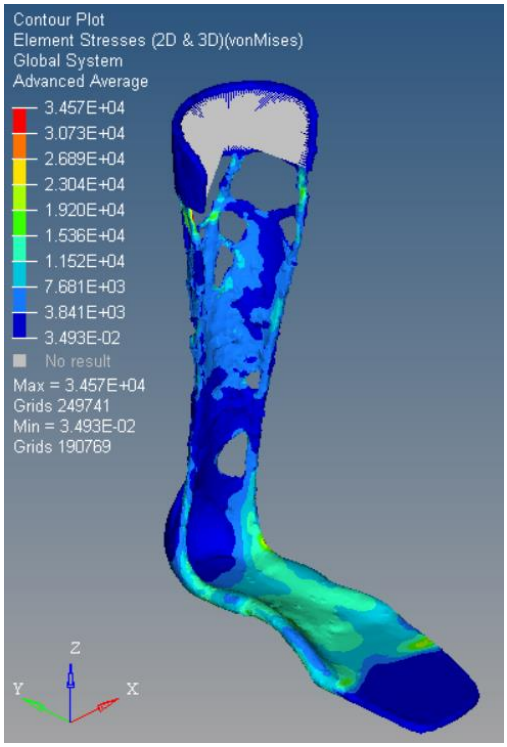

Figure 56: VonMises stress contour plot for FEA re-analysis in MPa on footplate torsion load case.

3.10 FINAL AFO DESIGN:

A SolidWorks render of the final AFO design is shown in Figure 57, which was smoothed out using Autodesk® Meshmixer™. The final design specifications are summarized in Table XVI.

Table XVI: Final AFO design specifications.

Design Model	DES4	
Material	Windform SP	
Strut Type	Posterior leaf spring	
Attachment Method	Velcro strap	
Overall Height	38.1	[cm]
Overall Width	9.5	[cm]
Overall Length	27.8	[cm]
Weight	575	[g]
Linear Stiffness of Strut	39	[N/mm]
Overall Linear Stiffness	1.88	[N/mm]
Strut Bending Stiffness	14.65	[N-m/deg]
Overall Bending Stiffness	4.01	[N-m/deg]
Approximate cost	3000	[$]

Figure 57: Final render of the posterior strut AFO design.

Table XVII and Table XVIII show additional performance data regarding linear and bending/rotational stiffness respectively for the final AFO design, based on the prescribed loading scenarios. Note that the significant spike in stiffness between the strut performance and overall performance is based on the fact that different boundary conditions are applied in either case. In terms of AFO performance, it is desirable that the overall stiffness is lower than the strut stiffness. This ensures that the strut is rigid and the majority of deflations are occurring due to MTP joint flection.

Table XVII: Linear deflection performance of the final AFO design.

Load Step	Applied Force [N]	Strut Linear Deflection [mm]	Linear Stiffness [N/mm]	Linear Stiffness [lb/in]
Heel Strike	37	5.4	6.85	39.1
Loading Response	45	6.6	6.82	38.9
Mid-Stance	53	7.8	6.79	38.8
Contralateral Heel Strike	83	44.2	1.88	10.7

Table XVIII: Bending/rotational deflection performance of the final AFO design.

Load Step	Applied Moment [N-m]	Angular Strut Deflection [deg]	Angular Stiffness [N-m/deg]	Angular Stiffness [lb-in/deg]
Heel Strike	12.95	0.88	14.65	0.130
Loading Response	15.75	1.08	14.58	0.129
Mid-Stance	18.55	1.28	14.53	0.129
Contralateral Heel Strike	29.05	7.24	4.01	0.036

The final design features were derived from the list of customer needs discussed in Appendix A section 1.1. These needs where divided into five main categories which are; AFO is functional, AFO is durable, AFO is safe, AFO is easily manufactural, patient needs and AFO is comfortable.

The AFO design met the patient's needs by being discreet and aesthetically pleasing. Ensuring that the AFO does not have any bulking geometry sticking out of the basic offset foot contour of the patient's foot achieved this.
We first started by importing a scanned cast model of the patient's foot, which was then used to define the foot contours of the AFO to ensure patient comfort. Moreover, the 3D model was then offset at vulnerable areas such as the ankle bone to ensure that the AFO does not cause any irritation or discomfort for the patient. We also ensured that the model was free of any sharp edges, so that the device does not cause harm to the patient.

For the AFO is functional category, we first defined that the AFO will help the patient simulate natural gate cycle. The AFO design does this by maximizing the forward propulsion, provide lateral stability, and keeping the patient's foot from dropping during the swing phase. The propulsion was maximized by incorporating the calculated stiffness target into the AFO design. The final AFO stiffness was achieved by optimizing the device's locations of deflection, the wall thicknesses and the locations and size cut outs where stresses were low. The design also had to accommodate for the fastening method which consisted of a Velcro strap that will be attached to the top section of the AFO.

4 CONCLUSION AND RECOMMENDATION

4.1 RECOMMENDATIONS

For the recommendations sections, details about how some of the processes for this project can be improved will be provided.

4.1.1 MATERIAL ANISOTROPY

The analytical approach to conducting topology optimization involved the assumption of isotropic material properties due to the lack of available material data provided by manufacturers. In the absence of adequate material testing, this approximation was the only option for the group. In reality, 3D printed materials behave anisotropically. Specifically, the material properties in the z-direction are different than the properties in

the x and y-directions due to the nature of the layer-by-layer process of building a part through additive manufacturing. Generally, the strength and stiffness in the z-direction is less than that of the x and y-directions for the process of 3D printing. This anisotropy is most notable in FDM, however it also exists to a lesser degree in SLS and Stereolithography processes. Furthermore, in FDM, the toolpath of the extruder nozzle and the infill pattern can also introduce anisotropy between x and y directions (in plane with the print bed). Another contributor to material anisotropy in 3D printed parts is attributed to thermal effects, and the heating and cooling of material, though this effect can sometimes be lessened in FDM by using a pre-heated print bed. The material properties in a 3D printed part are very process-dependent, and it is for this reason that a lot of material datasheets for these materials do not include a full description of the anisotropic behaviour of the material. The lack of material data further complicates the issue of accounting for material anisotropy in our analysis. It is for these reasons that our analysis makes the assumption of isotropic material properties. However, it is recommended to pursue an anisotropic analysis in the future, as this non-uniform behaviour can drastically change the performance of the design.

In the simplest case of isotropic material properties, the three-dimensional compliance matrix requires just three material properties to describe the material's elastic behaviour under load: Young's Modulus, Poisson's Ratio, and Shear Modulus. For an isotropic material, Poisson's Ratio and Shear Modulus are related through the following relation:

$$G = \frac{E}{2(1+v)}$$

For an isotropic material, Hook's Law describes the relationship between stress and strain for any direction as follows:

$$\begin{bmatrix} \varepsilon \\ \gamma \end{bmatrix} = \begin{bmatrix} \frac{1}{E} & -\frac{v}{E} \\ -\frac{v}{E} & \frac{1}{G} \end{bmatrix} \begin{bmatrix} \sigma \\ \tau \end{bmatrix}$$

The most complete description of an anisotropic material's three-dimensional stiffness characteristics requires 21 unique material properties. One approach for analyzing the anisotropy of 3D printed materials is to assume that the material is orthotropic, meaning that the material has three mutually orthogonal planes of symmetry. For an orthotropic material simplification there are only nine material properties needed to fully describe the stiffness matrix. For an orthotropic material, the stress tensor is as follows:

$$\begin{bmatrix}\varepsilon_{11}\\ \varepsilon_{22}\\ \varepsilon_{33}\\ \gamma_{23}\\ \gamma_{13}\\ \gamma_{12}\end{bmatrix}=\begin{bmatrix}\frac{1}{E_{11}} & -\frac{v_{21}}{E_{22}} & -\frac{v_{31}}{E_{33}} & 0 & 0 & 0\\ -\frac{v_{12}}{E_{11}} & \frac{1}{E_{22}} & -\frac{v_{32}}{E_{33}} & 0 & 0 & 0\\ -\frac{v_{13}}{E_{11}} & -\frac{v_{23}}{E_{22}} & \frac{1}{E_{33}} & 0 & 0 & 0\\ 0 & 0 & 0 & \frac{1}{G_{23}} & 0 & 0\\ 0 & 0 & 0 & 0 & \frac{1}{G_{23}} & 0\\ 0 & 0 & 0 & 0 & 0 & \frac{1}{G_{12}}\end{bmatrix}\begin{bmatrix}\sigma_{11}\\ \sigma_{22}\\ \sigma_{33}\\ \sigma_{23}\\ \sigma_{13}\\ \sigma_{12}\end{bmatrix}$$

It is obvious from the stiffness matrix for an orthotropic material that the stresses in one direction are influenced by the material properties in all other directions. Commonly, the case of a 3D printed material can be further simplified to a transversely isotropic scenario. This approach is valid under the assumption that the material properties in the 1 and 2 directions are the same, and requires that only five unique material properties be known in order to fully describe the behaviour of the material. Mathematically, the stress tensor is further simplified by the following [13]

$$E_{11} = E_{22}$$
$$v_{21} = v_{12}$$
$$v_{31} = v_{13}$$
$$v_{23} = v_{32}$$

In this case, the 3-3 direction would be equivalent to the z-direction of the 3D printer coordinates (or the layer direction), whereas 1-1 and 2-2 directions represent the x and y coordinates respectively. The approximation of transversely isotropic material properties would assume that the material properties in the x and y directions are equivalent, while the z direction has alternate material properties. This is the recommended approach for analyzing the anisotropic behavior of material properties, as it reduces the complexity of the analysis greatly, while still accounting for anisotropy in 3D printed materials due to layer direction.

Since most companies do not provide a full description of the anisotropic behavior of 3D printable polymers in their material data sheets, it is also recommended to perform

material testing which is adequate for describing the behavior in the x, y, and z directions and for determining the give independent material properties needed. Hyperworks has the capacity to handle transversely isotropic material properties in FEA and Topology Optimization studies using the MAT8 material card, so this approach would be compatible with the software's capabilities.

4.1.2 Non-Linear Geometry

For this report, topology optimization process was conducted using a linear-elastic solver method, which does not account for large strains or large deformations. For truly optimal propulsion characteristics of the AFO, it is desirable to have localized deformation concentrated at one particular region (in the case of this design, the MTP region). To achieve this, the ideal design would maximize compliance in the region intended for deflection, and minimize compliance in all other locations. However, maximizing compliance introduces high strain energy density, which in turn results in the linear-static approximation of Infinitesimal Strain Theory to become invalid. For large localized strains, terms in the Green-Lagrangian Strain Tensor that were previously small enough to be ignored begin to dominate the governing strain equations, and Finite Strain Theory is required to fully describe the behavior of the material. For this reason, a linear-elastic study in Hyperworks is not the ideal approach. Using linear elastic equations to describe non-linear behavior can be dangerous and can result in unrealistic and inaccurate results. Similarly, if the AFO material is not sufficiently stuff, a non-linear situation is encountered.

4.1.3 OpenSim

We recommend using OpenSim to simulate the patient's gate instead of Microsoft excel. OpenSim is a very powerful program that can be used as a kinematics and dynamics tool, to analyse the patient at the different stage of gate. OpenSim would also be able to determine all the joint's angle flections, reaction force at each joint and also determine the target stiffness of the AFO. we were unable to use OpenSim due to its complex learning curve, but if we did know how to use it our stiffness targeting would have been much easier to obtain.

4.1.4 MAXIMIZING AFO PROPULSION USING SHIMS

The implementation of a shim design will allow the patient to get the most out of the AFO, by maximizing its propulsion. The general idea behind the shim is it will cause the patient to lean into the AFO and increasing its the deflection angle, thereby increasing the potential energy of the device. Figure 58 below illustrates an exaggerated model of what the patent's leg/foot and AFO might look like without the implementation of a shim. Without the shim, there is no deflection at the knee or the MTP and the patent's weight will mostly be on his/her heel, meaning there will be no preload on the AFO during mid-stance. Figure 59 however, shows how the shim allows the patient to lean into the AFO, causing it to deflect at the hinge and store more energy, allowing for a higher energy return during push off [14].

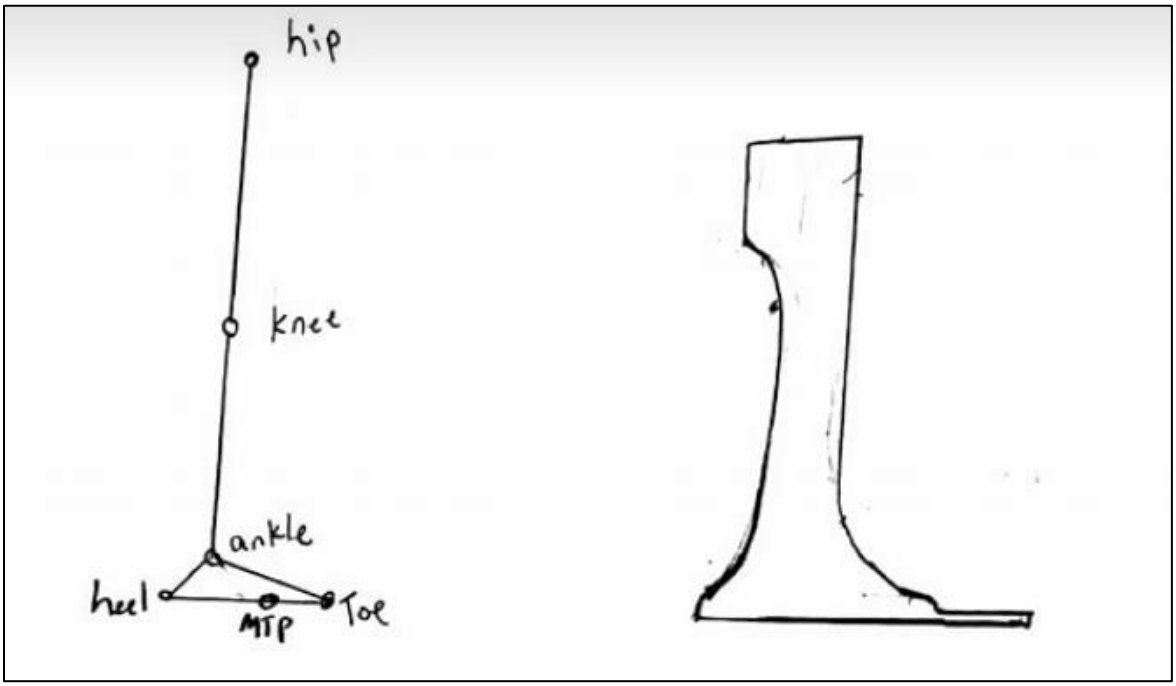

Figure 58: vertical leg without shim.

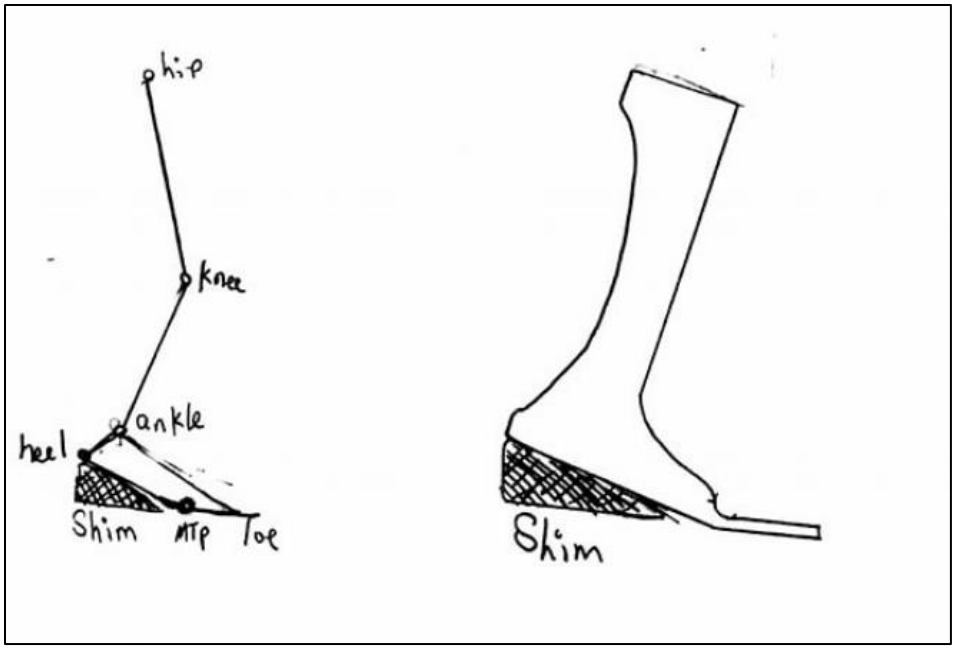

Figure 59: knee and AFO flexion with shim.

The shims have the same inside surface contours as the outside surface of the AFO, allowing the AFO to sit on the shim without shifting around. Likewise, the bottom side of the shim was designed to be flat so it can sit flush on the sole of the shoe without moving.

The maximum angle of elevation for the shim will be 3.2 degrees. At this angle, propulsion will be maximized and at the same time the patient will not feel fatigue in his/her quadriceps due to a larger knee deflection angle. Three shims should be used, with the 1.2, 2.2 and 3.2 degree elevation angles, which will be worn by the patient in a gradual manner, starting with the 1.2 degree shim then working up to the 3.2 degree shim. The gradual process will make it easier for the patient to adjust to the largest shim.

4.1.5 REMODELING OPTIMIZED DESIGN

We recommend finding a software that will be more user friendly for remodeling the optimized design to make it feasible. The models that are outputted by CANFIT where not easily inputted into Hyperworks because the model had too many tessellations to run

smoothly in the program. This meant that an additional step was required to reduce the tessellations before plugging the model into Hyperworks. The program that was used to undergo this intermediate step was called Geomagic. The model was then plugged into Hyperworks for meshing, FEA and topology optimization, after which it was inputted into Meshmixer to create a smooth surface model. After change and smoothing the surface the FEA had to be reran using Hyperworks. After the smoothing and FEA step was complete, the model was plugged into SolidWorks to create the final rendering. Figure 60: Modeling programs and processes flow chart. Figure 60 shows the process and programs used in a flow chart.

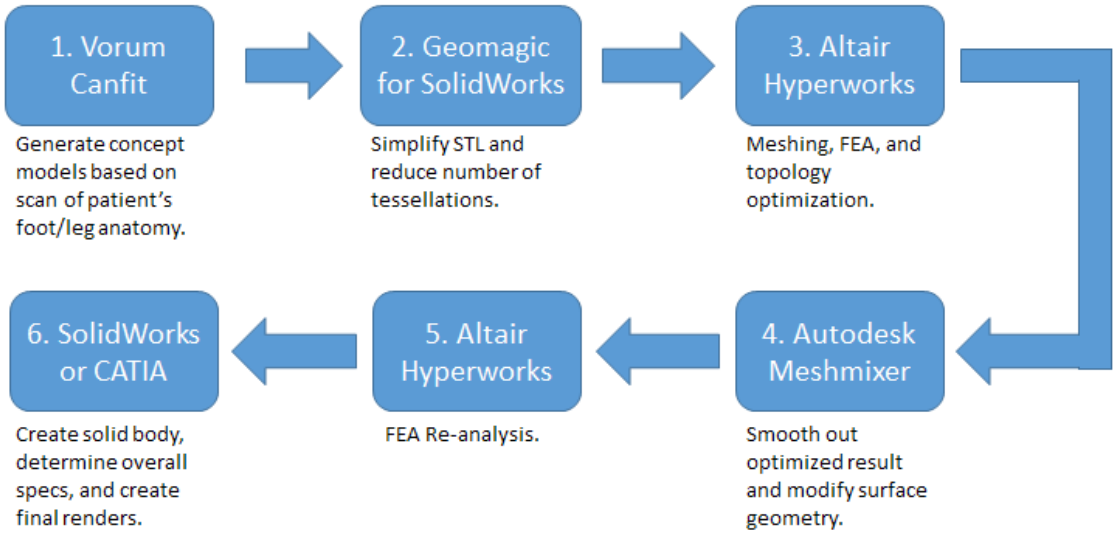

Figure 60: Modeling programs and processes flow chart.

4.1.6 Motion Capture Process Improvements

Some recommendations for the motion capture process which will help eliminate the source of error, include having a touchless video recording actuator for the camera and not touching the camera after it has been set up for recording. During the motion capture session, the camera was first set up, and then the video button on the camera is pressed after the patent was ready for the recording. When the bottom is pressed, the camera will slightly move/ change view angles which introduced a source of error in the data collection. A good way to avoid this is to first set up the camera, then having a separate remote to actuate the video recording once the patent was ready. Doing so, will

illuminate any shifting or movement in the camera which will produce a more consistent data collection.

The gait kinematics of the patient are mechanically assessed using a straightforward motion capture approach. Motion capture methodology should be similar to that which is detailed in section 2.2.1 with a focus on limiting distortion of data points due to depth of field. A camera with high focal length is recommended for image flattening and increased data precision. In capturing new patient data, it is recommended that GRF data is collected simultaneously, if possible. Data matching of the kinematic motion to the dynamic pressure data has an impact on the precision of muscle moment calculations. If possible, data filtration should be applied to all collected data points so that the center of pressure (COP) distribution and joint displacements follow smooth sinusoidal motion patterns that would be expected of patient motion. It is noted that only 2-dimensional sagittal plane displacement of the patient is necessary for this pendulum-model adapted design method, but a multiple camera setup would still be desirable for data precision.

The motion capture data processing is conducted on Adobe® After Effects, although other commercial methods are available. Careful attention should be drawn to tracking jitter that occurs in automatic data point tracking in After Effects.

Our team also recommends the use of a raised walking platform to be used in conjunction with the Wii-Fit Board for obtaining GRF data, with a cut-out that will allow the Wii-fit to sit flush with the platform surface. The Wii-Fit Board that was used to collect the GRF data, was not flush with the ground, so patient had to step up onto the plate which did not mimic a natural gate cycle on flat ground. This might have generated a source of error in our data collection and this error could have been avoided if the surface of the Wii-fit was in line with the ground.

4.1.7 Exploring an Assembly Approach

We also recommend using an assembly for the AFO design instead of using a single component. The single component is unable to deflect the amount that we needed it to bend at the MTP because the material will fail due to the high elongation. So, in order for

the single component design to work without breaking, we designed it to deflect a small amount in various areas. This was undesirable, because if the AFO deflects in more than one location it will simulate two or more springs in series, which will decrease the stiffness of the AFO significantly. Therefore, if we used an assembly approach, the single hinge with a torsional spring or leaf spring design could have been implemented, which would have made the analysis much simpler and allowed the AFO to maximize propulsion.

4.1.8 User friendly remodeling

Some recommendations for the motion capture process which will help eliminate the source of error, include having a touchless video recording actuator for the camera and not touching the camera after it has been set up for recording. During the motion capture session, the camera was first set up, and then the video button on the camera is pressed after the patent was ready for the recording. When the bottom is pressed, the camera will slightly move/ change view angles which introduced a source of error in the data collection. A good way to avoid this is to first set up the camera, then having a separate remote to actuate the video recording once the patent was ready. Doing so, will illuminate any shifting or movement in the camera which will produce a more consistent data collection.

4.1.9 Load Application and Boundary Conditions:

To simplify the analysis, there is assumed perfect rigidity between the contact patches of the heel and/or toe, depending on center of pressure location, rather than real contact interaction between the AFO, the foot, and the shoe. Contact influences boundary condition behavior in FEM, but is very intensive to correctly model. The assumption that there are minimal energy losses between surfaces of the AFO and its surroundings are acceptable because the sole of a shoe can generally deform when subjected to loading, so it is not likely that high dynamic friction forces will be acting on the AFO. The deformation will have slight effects on patient kinematic behavior due to kinetic losses but this is considered negligible, as a shoe generally does not noticeably increase energy input required to walk.

4.1.10 PATIENT-SPECIFIC CUSTOMIZABLE DESIGN APPROACH

The approach of this design sets up the analytical methodology that can be modified for multiple patients based on their gait constraints. Rather than producing multiple sizing options, it is more advantageous to individualize the designs to fit locomotive limitations. The process of modifying the design involves the following components:

1. Patient diagnostics
2. Patient imaging
3. Data parsing and model inputs
4. Parameterization
5. Post processing
6. Fitting and adjustments

4.1.10.1 PATIENT DIAGNOSTICS

The patient's muscular range must be assessed, along with any specific concerns related to lifestyle activity that can affect the stiffness constraints of the optimized device. This process follows the standard procedure typical of AFO prescription to the patient. Along with this procedure, it is very important that accurate ground reaction force (GRF) data is obtained for the patient's weakened leg. This data is foundational to the stiffness targeting of the adapted device. A Nintendo Wii® balance board can be used to capture vertical-axis GRF data, and planar pressure distribution from strain gage deformations, but a commercial device is recommended for its ability to capture horizontal-axis GRF data. The horizontal-axis GRF information is derived in the mathematical model utilized in this report, but it is always advisable to use accurate experimental data where possible.

4.1.10.2 PATIENT IMAGING

The gait kinematics of the patient are mechanically assessed using a straightforward motion capture approach. Motion capture methodology should follow the method conducted herein, with a focus on limiting distortion of data points due to depth of field. A camera with high focal length is recommended for image flattening and increased data precision. In capturing new patient data, it is recommended that GRF data is collected

simultaneously, if possible. Data matching of the kinematic motion to the dynamic pressure data has an impact on the precision of muscle moment calculations. If possible, data filtration should be applied to all collected data points so that the center of pressure (COP) distribution and joint displacements follow smooth sinusoidal motion patterns that would be expected of patient motion. It is noted that only 2-dimensional sagittal plane displacement of the patient is necessary for this pendulum-model adapted design method, but a multiple camera setup would still be desirable for data precision.

The motion capture data processing is conducted on Adobe® After Effects, although other commercial methods are available. Careful attention should be drawn to tracking jitter that occurs in automatic data point tracking in After Effects. Figure XXX depicts this possible oscillation, and the effect is a fluctuation in joint segment acceleration values calculated that are detrimental to the subsequent AFO load calculations.

The kinematic model has several indicated inputs. The ideal mathematical approach follows a pseudo-inverse kinematics approach. Generally, the patient's gait is disassembled into a series of required muscle moments, and is used to diagnose mechanical constraints in a quantifiable sense. These constraints are then compared to an idealized model of optimal gait, and with proper input of the patient's dimensions, a series of load conditions and stiffness behavior of a properly fitted AFO are generated.

4.1.10.3 TEST DATA

The design approach used within the constraints of this project utilized low-cost test and analysis methods whenever possible. This can create difficulty in turnaround time of the device strictly due to the availability of software necessary to turn collected data into a finished product. The parsing of GRF data occurs using OSC signal reading software, and the data is converted to physical force magnitudes and vector directions using a custom VBA script. This approach served well within the time constraints of the design process, but it is recommended that, in absence of access to a commercial force plate with simple data collection, a MatLab script be written to collect GRF data from the Bluetooth signal of the balance board, filter the data, and tabulate it. The script could then be incorporated into a more mathematically rigorous iterative solver approach to inverse kinematics. Once this step is completed, the data can be paired with the motion

capture plot to input into the kinematic/dynamic model template.

4.1.10.4 PARAMETERIZED AFO MODEL

Creating a parameterized model for the AFO design space would allow for significantly more customization and refinement of the final design. One of the largest obstacles faced by the group was the time-consuming and difficult modelling task associated with making modifications to the AFO model. It was determined that further modification of the AFO design could be achieved through revisiting the initial design space generated in Canfit, and modifying certain parameters of the initial design. Since the topology optimization results are limited by the initial design space, having a simpler method of editing design space geometry would have been beneficial both in terms of time-savings, and overall quality of results obtained. The process for generating the concept models involved using Canfit to create a three-dimensional design space. Canfit is very user-friendly and easy to use, however it has some significant drawbacks.

Currently, Canfit does not have the ability to create variable thickness surface offsets. This meant that only constant thickness AFO concept designs could be achieved through modelling in Canfit. However, a variable thickness concept model is desirable, as certain regions of the AFO are more restricted by shoe fitment (specifically the footplate region), and are therefore limited to smaller thickness constraints than the strut, which can be of larger thickness. Furthermore, it was found that after the topology optimization study was conducted to determine the optimal geometry for a given material, it was difficult to apply similar geometry to another model of a different material without re-running the optimization study, which is both time consuming and resource intensive. Additionally, optimization studies for weaker materials would fail due to inadequate initial geometry of the design space, which was generated in Canfit, and was difficult to edit once it was already in Hyperworks. Finally, Canfit only has the capability to export models as STLs, which are difficult to work with in other solid modelling CAD systems like SolidWorks or CATIA, and must be converted to a more universal CAD format like STEP or IGES.

All of the issues that arose from using Canfit as the primary modelling software could be alleviated if a parameterized CAD model was created. A parameterized model is one whose features are editable through parametric relationships and equations built into the CAD modelling software. This is common modelling practice, and is particularly beneficial when quick edits are desired for a particular part. With a parameterized model, simply inputting dimensions into a text field can automatically apply the necessary changes to part geometry, rather than having to re-build the model from the ground up every time a moderate part geometry modification is required. Creating a parameterized model would be a time-consuming process upfront, but would result in significant time savings during the finishing stages of the optimization process, and would allow for more versatility and customization of the finished design. In contrast, our team had to rely on the topology optimization results to output geometry that was both functional and feasible. A parameterized model would allow for an easy transition between a rough topology optimized result and a finished print-ready design.

4.1.10.5 ITERATIVE TOPOLOGY OPTIMIZATION

As mentioned previously, it was found that for most materials the initial design space model was not adequate to produce a feasible topology optimization result, whether due to artificially imposed stress concentrations or due to excessive deflections which cause the model to transition into the realm of non-linear geometry (large deflections). Topology optimization is iterative by definition, as the code iteratively varies geometry until it converges on a solution based on the user's inputs and parameters. However, the process itself must also be iterative in order to achieve a fully optimized design that meets all required needs, targets, and specifications. This means that once an initial topology optimization result is achieved, it is necessary to interpret and learn from the results obtained, and use them to modify the initial design space (optimization starting point). This will ensure that the next iteration of topology optimization will be more likely to obtain the desired results.

Due to significant time constraints, the group was not able to adequately follow through with the full optimization approach. The team achieved one iteration of topology optimization, and then applied the results to create a 3D print-ready AFO design. However, it became apparent after the first successful attempt at topology optimization

that further iterations would be necessary to obtain a truly optimized design. In the future it is recommended that adequate time be allocated to running multiple iterations of topology optimization and refinement. If this recommendation is followed, it is likely that a feasible solution can be achieved using a much more affordable and readily available material such as PC-ISO or Ultem 9085.

4.1.10.6 Data Parsing and Model Inputs

The design approach used within the constraints of this project utilized low-cost test and analysis methods whenever possible. This can create difficulty in turnaround time of the device strictly due to the availability of software necessary to turn collected data into a finished product. The parsing of GRF data occurs using OSC signal reading software, and the data is converted to physical force magnitudes and vector directions using a custom VBA script. This approach served well within the time constraints of the design process, but it is recommended that, in absence of access to a commercial force plate with simple data collection, a MATLAB script be written to collect GRF data from the Bluetooth signal of the balance board, filter the data, and tabulate it. The script could then be incorporated into a more mathematically rigorous iterative solver approach to inverse kinematics.

4.2 Conclusion

In conclusion, this report outlines the preferred design process for a 3D-printable ankle-foot orthosis (AFO) in partnership with Anderson Orthopedics. The project objective was to design a prototype that could improve gait and maximize forward propulsion, while providing quantifiable justification of critical design choices. The design is aimed to last at least two years, while being comfortable for the patient.

First, the team collected motion capture data and analyzed gait kinematics in order to quantify patient locomotive characteristics. The team then used this data to determine design targets for optimization of the AFO. Finally, the team used topology optimization techniques to achieve a quantifiably propulsion-aiding device.

The optimizations process was carried through for two design concepts, an improved iteration of the initial prototype, and a more geometrically complex concept. It was determined that the optimal choice was a modification of the previous prototype. The newly developed iteration was able to meet functional needs, albeit its torsional stiffness of 4.1 Nm/deg would mean a suboptimal propulsion gain. The final design achieved a factor of safety of 1.33.

The failure mode and effect analysis (FMEA) and determined that the heel raise/ toe push off process was the most critical. This was because the heel raise/toe push off process had the highest number of failure modes and the highest RPN value of 243 for the fatigue at the hinge failure mode.

A fatigue failure analysis was conducted to determine the maximum fatigue stress for a life cycle of two year or 5,000,000 cycles. The maximum fatigue stress for PLA was determined to be 2.52 MPa. The S-N curve was not attainable for the material that was used for the AFO design therefore, this analysis was used to illustrate the process of determining the fatigue stress.

REFERENCES

[1] NHS Health Quality, "Use of ankle-foot orthoses following stroke," NHS Quality Improvement Scotland, Edinburgh, Glasgow, 2009.

[2] D. B. M. v. d. K. V. G. J. H. M. S. Collins, "The effect of ankle foot orthosis stiffness on the energy cost of walking: a simulation study," *Clinical Biomechanics,* 2011.

[3] v. Campbell, "Risk Assessment and Mitigation: Failure Modes and Effects Analysis (FMEA)," 15 Oct 2017. [Online]. Available: http://home.cc.umanitoba.ca/~labossip/4860/Presentations.html,.

[4] D. G. Ullman, the mechanical design process second edition, Oregon state university, 2015.

[5] "Mean Stress Effects," 08 Nov 2016. [Online]. Available: http://www.ux.uis.no/~hirpa/KdB/ME/S-N%20diagram.pdf.. [Accessed 18 Nov 2017].

[6] R. K. Srinivasan, "characterization and testing of 3D printed sprockets," Westlake High School, 27 Jan 2016. [Online]. Available: https://sffsymposium.engr.utexas.edu/sites/default/files/2016/143-Srinivasan.pdf. [Accessed 14 Nov 2017].

[7] 3DXTECH, "Technical data," 3DXTECH, 2017. [Online]. Available: https://www.3dxtech.com/technical-data/. [Accessed 6 dec 2017].

[8] CIMETRIX, "Stratasys F123 Series," [Online]. Available: http://www.cimetrixsolutions.com. [Accessed 21 10 2017].

[9] CRP Technology, "Windform," CRP, 2016. [Online]. Available: http://www.crptechnology.com/windform-3d-printing-materials/. [Accessed 6 dec 2017].

[10] Javelin, "Biocompatible mateial with superior strength," Javelin, 2017. [Online]. Available: http://www.javelin-tech.com/3d-printer/materials/fdm-thermoplastic/pc-iso/. [Accessed 06 dec 2017].

[11] Stratasys Ltd., "FDM Thermoplastics," [Online]. Available: http://www.stratasys.com/materials/fdm. [Accessed 20 10 2017].

[12] Herff College of Engineering, "Plane Stress/Strain Equations," University of Memphis, 2015. [Online]. Available:

http://www.ce.memphis.edu/7117/notes/presentations/chapter_06a.pdf. [Accessed 5 December 2017].

[13] M. E. Tuttle, Structural analysis of Polymeric composite materials, CEC press Taylor & Francis group.

[14] E. O. Mr Kavi C. Jagadamma, "The effects if tuning an ankle-foot orthosis footwear combination on kinematics and kinetics of the knee joint of an adualt with hemiplegia," Prosthetics and Orthotics International , 1 Sept 2010. [Online]. Available: http://journals.sagepub.com/doi/10.3109/03093646.2010.503225. [Accessed 18 Nov 2017].

[15] "Wear Resistnace," IWIS, 2016. [Online]. Available: http://www.iwis.de/en/drive-systems/chain-engineering/chain-basics/wear-resistance/. [Accessed 25 03 2016].

[16] J. H. Wynne, "Orthotic Device and Method". United Kingdom Patent 2811705, 21 September 2011.

[17] S. Willner and K. Engdahl, "Ankle-Foot Orthosis". Sweden Patent 2279225, 10 July 1997.

[18] D. Totah, I. Kovalenko, M. Saez and K. Barton, "Manufacturing Choices for Ankle-Foot Orthoses: A Multi-objective Optimization," *Procedia CIRP,* vol. 65, no. 2017, pp. 145-150, 2017.

[19] J. F. A. Smits, "Ankle-Foot Orthosis". Netherlands Patent 2444263, 18 April 2002.

[20] S. W. Nickson, "Ankle/Foot Orthosis". United Kingdom Patent 2422734, 8 November 2000.

[21] A. T. Ingimundarson, O. Olafsson, A. V. Clausen and K. O. V. De Roy, "Ankle-Foot Orthosis". Iceland Patent 2502680, 7 November 2003.

[22] F. Hempel, Z. Javed, C. McKenzie and M. Wu, "Final Design Report: BIA," University of Manitoba, Winnipeg, 2016.

[23] C. R. Ethier and C. A. Simmons, Introductory Biomechanics: From Cells to Organisms, Cambridge: Cambridge University Press, 2007.

[24] M. Alam, I. A. Choudhury and A. B. Mamat, "Mechanism and Design Analysis of Articulated Ankle Foot Orthoses for Drop-Foot," *The Scientific World Journal,* vol. 2014, no. 2014, p. 14, 2014.

[25] U. F. a. D. Administration, "CFR - Code of Federal Regulations 21," US Department of Health and Human Services, 1 April 2017. [Online]. Available: https://www.accessdata.fda.gov/scripts/cdrh/cfdocs/cfcfr/CFRSearch.cfm?fr=820.198. [Accessed 27 October 2017].

[26] US Food and Drug Administration, "Product Classification - Device: Joint, Ankle, External Brace," US Department of Health and Human Services, 23 October 2017. [Online]. Available: https://www.accessdata.fda.gov/scripts/cdrh/cfdocs/cfpcd/classification.cfm?ID=5055. [Accessed 26 October 2017].

[27] Smart & Biggar Fetherstonhaugh, "Patent protection for medical inventions in various jurisdictions," 18 May 2012. [Online]. Available: http://www.smart-biggar.ca/en/articles_detail.cfm?news_id=608. [Accessed 20 October 2017].

[28] Government of Canada, "Medical Device Regulations - SOR/98-282 Food and Drugs Act," 13 October 2017. [Online]. Available: http://laws-lois.justice.gc.ca/eng/regulations/sor-98-282/FullText.html. [Accessed 26 October 2017].

[29] Emergo, "Health Canada Regulatory Approval Process for Medical Devices," UL, 2017. [Online]. Available: https://www.emergogroup.com/resources/canada-process-chart. [Accessed 20 October 2017].

[30] US Food and Drug Administration, "Facts About the Current Good Manufacturing Practices (CGMP)," US Department of Health and Human Resources, 6 October 2017. [Online]. Available: https://www.fda.gov/drugs/developmentapprovalprocess/manufacturing/ucm169105.htm. [Accessed 27 October 2017].

[31] US Food and Drug Administration, "CFR - Code of Federal Regulations Title 21," US Department of Health and Human Services, 1 April 2017. [Online]. Available: https://www.accessdata.fda.gov/scripts/cdrh/cfdocs/cfcfr/CFRSearch.cfm?fr=820.180. [Accessed 27 October 2017].

[32] Cascade Orothotics Ltd, "Ankle-Foot Orthosis (AFO)," 2017. [Online]. Available: http://www.cascadeorthotics.com/ankle-foot-orthosis-afo-cascade-orthotics/. [Accessed 20 10 2017].

[33] E. T. Esfahani, Developing an active ankle foot orthosis based on shape memory alloys, Toledo: University of Toledo, 2007.

[34] P. Figari, "Steps tp Analyzing a Material's Properties From Its Stress.Strain Curve," 08 09 2015. [Online]. Available: http://www.instructables.com/id/Steps-to-Analyzing-a-Materials-Properties-from-its/. [Accessed 20 10 2017].

[35] A. G. B. L. Z. A. Matt Wallis, "Development of Ankle-Foot Orthosis Design," winnipeg, 2017.

[36] Intertek, "Izod Impact (Notched) ASTM D256, ISK180," [Online]. Available: http://www.intertek.com/polymers/testlopedia/notched-izod-impact-astm-d256/. [Accessed 20 10 2017].

[37] Eastman Amphora, "Technical Data Sheet EastmanAmphora 3D Polymer Am1800," 30 08 2014. [Online]. Available: http://ws.eastman.com/ProductCatalogApps/PageControllers/ProdDatasheet_PC.aspx?Product=71100831&sCategoryName=Generic#_ga=2.85851420.405205414.1508308823-769849811.1507247874. [Accessed 21 10 2017].

[38] Eastman Amphora, "Technical Data Sheet Eastman Amphora 3D Polymer AM3300," 10 11 2015. [Online]. Available: http://ws.eastman.com/ProductCatalogApps/PageControllers/ProdDatasheet_PC.aspx?Product=71104597&sCategoryName=Generic#_ga=2.52992301.405205414.1508308823-769849811.1507247874. [Accessed 21 10 2017].

[39] Boedeker Plastics Inc., "PEEK (PolyEtherEtherKetone) Specifications," [Online]. Available: http://www.boedeker.com/peek_p.htm. [Accessed 21 10 2017].

[40] Boedeker Plastics Inc., "Spectar PETG (PolyEthleneTerephtalate Glycol Copolyester) Specifications," [Online]. Available: http://www.boedeker.com/spectar.htm. [Accessed 21 10 2017].

[41] WS Hampshire Inc., "ACETAL," [Online]. Available: http://www.wshampshire.com/pdf/acetal_grades.pdf. [Accessed 21 10 2017].

[42] LULZBOT, "Printers," [Online]. Available: https://www.lulzbot.com/store/printers. [Accessed 21 10 2017].

[43] Proto3000, "Professional 3D Printers," [Online]. Available: https://proto3000.com. [Accessed 22 10 2017].

[44] RehabMart, "Ankle Foot Orthosis, MultiPodus Boots, Foot Drop, AFO," [Online]. Available: https://www.rehabmart.com/category/afo_multi_podus.htm. [Accessed 22 10 2017].

[45] Precision ADM, "Advanced Digital Manufacturing," [Online]. Available: www.precisionadm.com. [Accessed 22 10 2017].

[46] P. Beer and R. Johnson, Mechanics of Materials, New York City: McGraw Hill Education, 2016.

[47] Stratasys, "Fortus 900mc Specifications," Stratasys, 2017. [Online]. Available: http://www.stratasys.com/3d-printers/fortus-900mc. [Accessed 5 12 2017].

[48] R. P. Institute, "Intro to Finite Elements," 2015. [Online]. [Accessed 5 December 2017].

[49] J. J. T. D. D. F. M. Ferdinard P. Beer E. Russell Johnston, Mechanics of materials 6th ed.

[50] Altair HyperWorks, "HyperMesh Desktop Introduction".

[51] Altair HyperWorks, "Optistruct Reference Guide".

[52] C. L. V. B. L. D. J. C. O'Connor, Dynamics of human gait, Cape town, South Africa: Kiboho Publishers.

[53] M. C. Hawkins, Experimental and computational analysis of an energy storage composite ankle foot orthosis, las vegas: university of nevada, 2010.

[54] D. P. N. Kolkata, "Objective analysis of kinetics and knematics parameters in gait".

[55] Altair University, "Practical aspects of finite element simulation," 2015.

[56] B. Gwynedd, "The importance of being earnest about shank and thigh kinematics especially," 1997.

[57] J. Z. X. S. B. Liu, "Standardized compliance matrixes for general anisotropic materials and a simple measure of anistropy degree based on shear-extension coupling coefficient," CNMM department of engineering mechanics, 1995.

[58] K. C. C. J. E. G. a. R. D. Draper, "additive manufacturing and characterization of ultem polymers and composites," NASA glenn research center, Cleveland, OH, 2015.